ATLAS NOTE

ATLAS-CONF-2014-058

September 30, 2014

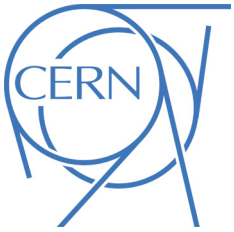

Estimation of non-prompt and fake lepton backgrounds in final states with top quarks produced in proton-proton collisions at $\sqrt{s}$=8 TeV with the ATLAS detector

The ATLAS Collaboration

Abstract

This note presents methods for estimating non-prompt and fake lepton backgrounds developed in the context of top analyses using the ATLAS detector. The analysis is performed on the ATLAS 2012 proton-proton collision data sample, collected at the LHC, corresponding to a luminosity of 20.3 fb^{-1} at $\sqrt{s}$=8 TeV. Final states with lepton+jets and dilepton events are considered. Two different data-driven methods are described and compared. The first method (matrix method) is based on the measurement of efficiencies of leptons with relaxed identification criteria. The second one (fitting method) is based on the construction of templates for non-prompt and fake leptons. For final states with two leptons, the systematic uncertainties of the estimates using the matrix method are 30-100%. For final states with one lepton, the two methods give consistent results within systematic uncertainties, which are 10-50% for the matrix method and 50% for the fitting method.

ATLAS-CONF-2014-058
01 October 2014

1 Introduction

The selection of events with top quarks is often based on the identification of one or more charged isolated leptons from the decay of W or Z bosons, referred to as 'prompt' or 'real' leptons in the following. Acceptance, quality and isolation requirements are applied to select these leptons.

Non-prompt leptons and non-leptonic particles may satisfy these selection criteria, giving rise to so called 'non-prompt and fake' lepton backgrounds. In the case of electrons, these include contributions from semileptonic decays of b- and c-quarks, photon conversions and jets with large electromagnetic energy (from the hadronisation to π^0's or from early showering in the calorimeter). Non-prompt or fake muons can originate from semileptonic decays of b- and c-quarks, from charged hadron decays in the tracking volume or in hadronic showers, or from punch-through particles emerging from high-energy hadronic showers. For analyses based on events with one lepton, this background stems from multi-jet events, characterised by a cross-section several orders of magnitude larger than for W boson or top events. In events with two leptons the non-prompt and fake lepton backgrounds are dominated by W+jets and semileptonic $t\bar{t}$ events, with a fake lepton in addition to the real one, and more rarely events with two fake leptons.

These backgrounds are estimated using data-driven techniques. The most common methods are called matrix, jet-lepton and anti-lepton methods (these latter two are referred to in the following as 'fitting methods') and have been used for ATLAS early top quark studies [1, 2]. All these techniques were also applied on more recent 7 TeV analyses in $t\bar{t}$ dilepton studies [3] or single top measurements [4]. This note presents a survey of these methods and their application with 8 TeV data. New methods are also developed in the context of $t\bar{t}$ dilepton analyses with 8 TeV data [5, 6].

Results are presented on typical top selections such as the $t\bar{t}$ semileptonic and the dileptonic selections. The analysis is performed in the ATLAS 2012 proton-proton collision data sample, corresponding to an integrated luminosity of 20.3 fb^{-1} at $\sqrt{s}$=8 TeV.

2 The ATLAS detector

The ATLAS detector [7] consists of four main subsystems: an inner tracking system surrounded by a superconducting solenoid, electromagnetic and hadronic calorimeters, and a muon spectrometer. The inner detector provides tracking information from pixel and silicon microstrip detectors in the pseudo-rapidity[1] range $|\eta| < 2.5$ and from a transition radiation tracker (TRT) covering $|\eta| < 2.0$, all immersed in a 2 T magnetic field provided by a superconducting solenoid. The electromagnetic (EM) sampling calorimeter uses lead and liquid argon (LAr) and is divided into a barrel region ($|\eta| < 1.475$) and an end-cap region ($1.375 < |\eta| < 3.2$). Hadron calorimetry is based on two different detector technologies, with scintillator tiles or LAr as active media, and with either steel, copper, or tungsten as the absorber material. The calorimeters cover $|\eta| < 4.9$. The muon spectrometer measures the deflection of muon tracks within $|\eta| < 2.7$ using multiple layers of high-precision tracking chambers located in toroidal fields of approximately 0.5 T and 1 T in the central and end-cap regions of ATLAS, respectively. The muon spectrometer is also instrumented with separate trigger chambers covering $|\eta| < 2.4$.

[1] ATLAS uses a right-handed coordinate system with its origin at the nominal interaction point (IP) in the centre of the detector and the z-axis coinciding with the axis of the beam pipe. The x-axis points from the IP to the centre of the LHC ring, and the y-axis points upward. Cylindrical coordinates (r,ϕ) are used in the transverse plane, ϕ being the azimuthal angle around the beam pipe. The pseudorapidity is defined in terms of the polar angle θ as $\eta = -\ln\theta/2$. For the purpose of the fiducial selection, this is calculated relative to the geometric centre of the detector; otherwise, it is relative to the reconstructed primary vertex of each event.

3 Simulation samples

Various Monte Carlo (MC) samples are used in the analysis. Simulated $t\bar{t}$ events are generated using the POWHEG generator v1_r2129 [8, 9], which implements the NLO matrix element for inclusive $t\bar{t}$ production, with the HERAPDF15NLO [10] parton distribution functions (PDFs). POWHEG is interfaced to PYTHIA v6.425 [11] with the CTEQ6L1 PDF set and the corresponding Perugia2011C tune [12]. The renormalisation and factorisation scales [13] are calculated event-by-event using $Q^2 = m_t^2 + p_{\mathrm{T}}^2$, where m_t and p_{T} are the top quark mass and the top quark transverse momentum. The top quark mass is assumed to be 172.5 GeV. Another $t\bar{t}$ sample, used for studies of systematic uncertainties, uses CT10 [14] PDFs. PYTHIA v6.425 with the AUET2B tune [15] is used for hadronisation and to describe the underlying event. The $t\bar{t}$ cross-section for pp collisions at a centre-of-mass energy of $\sqrt{s} = 8$ TeV is $\sigma_{t\bar{t}} = 253^{+15}_{-16}$ pb. It has been calculated at next-to-next-to leading order (NNLO) in QCD including resummation of next-to-next-to-leading logarithmic (NNLL) soft gluon terms with top++2.0 [16–22]. The PDF and α_S uncertainties were calculated using the PDF4LHC prescription [23] with the MSTW2008 68% CL NNLO [24,25], CT10 NNLO [14,26] and NNPDF2.3 5f FFN [27] PDF sets and these are added in quadrature to the scale uncertainty.

Table 1: A summary of generators, PDF sets and cross-section calculations used for the various simulated samples used in the analysis.

Process	Generator	PDF	Tune	Shower	Normalisation
$t\bar{t}$	POWHEG	HERAPDF15NLO	P2011C	PYTHIA 6.427	NNLO+NNLL
t (t-channel)	AcerMC	CTEQ6L1	P2011C	PYTHIA 6.425	NLO+NNLL
t (s-,Wt-channel)	POWHEG	CT10	P2011C	PYTHIA 6.425	NLO+NNLL
$t\bar{t}WW$+jets	MADGRAPH	CTEQ6L1	P2011C	PYTHIA 6.425	NLO
$t\bar{t}W/Z$+jets	ALPGEN	CTEQ6L1	AUET2	HERWIG 6.520.2	NLO
W+jets	ALPGEN	CTEQ6L1	P2011C	PYTHIA 6.426	NNLO
Z+jets	ALPGEN	CTEQ6L1	P2011C	PYTHIA 6.426	NNLO
$WW/WZ/ZZ$	ALPGEN	CTEQ6L1	AUET2	HERWIG 6.520.2	NLO
di-jet	PYHTIA	CTEQ6L1	AU2	PYTHIA 8	LO

Samples of single top quark backgrounds corresponding to the s-channel and Wt production mechanisms are generated with POWHEG using the CT10 set of PDF, while for the t-channel AcerMC [28] using the CTEQ6L1 set of PDF. All samples are interfaced to PYTHIA set of PDF and Perugia P2011C tune. Overlaps between the $t\bar{t}$ and Wt final states are removed using the so-called diagram removal scheme [29]. The single top quark cross-sections are normalised to the approximate NLO+NNLL QCD cross-sections [30, 31] using the MSTW2008 NNLO PDF.

Samples of W/Z+jet events are generated using the ALPGEN v2.14 [32] LO generator and the CTEQ6L1 PDF set [33]. Parton shower and fragmentation are modeled with PYTHIA v6.425. To avoid double-counting of partonic configurations generated by both the matrix-element calculation and the parton-shower evolution, a parton-jet matching scheme (MLM matching) [34] is employed. The W/Z+jet samples are generated with up to five additional partons, separately for W/Z+ light jets, W/Z+ $b\bar{b}$+jets and W/Z+ $c\bar{c}$+jets. The overlap between $W/Z+Q\bar{Q}(Q = b, c)$ events generated from the matrix element calculation and those generated from parton-shower evolution in the W/Z+light jet samples is avoided via an algorithm based on the angular separation between the extra heavy-quarks: if $\Delta R(Q, \bar{Q}) > 0.4$, the matrix-element prediction is used, otherwise the parton-shower prediction is used. For assessment of systematic uncertainties, W/Z+jet samples are also generated using SHERPA v1.4.1 [35], for the hard process, the parton shower and hadronisation, and the underlying event, with the CT10 PDF set. The

inclusive cross-sections of W/Z-boson production are calculated to NNLO with FEWZ [36] with an uncertainty of ±4%. For the W+jets and Z+jets backgrounds in association with two additional jets the uncertainty is conservatively estimated from the Berends-Giele scaling [37, 38] (W+n+1/W+n) and this yields ±34%

The ZZ/γ^*, WZ/γ^* and WW+jets samples are generated using `ALPGEN+HERWIG` with up to three additional partons. They are normalised to the NLO QCD cross-section prediction using the MSTW2008NLO set.

The samples of $t\bar{t}$+Z(+jets) and $t\bar{t}$+W(+jets) production are generated with `ALPGEN` with AUET2 tune, while the $t\bar{t}$+WW sample is generated with `MADGRAPH` [39] interfaced to `PYTHIA` with CTEQ6L1 PDFs. They are normalised to NLO cross-section predictions [6].

A sample of di-jet events is also used in the following, to derive one of the templates for the non-prompt and fake lepton background and to perform MC-simulation based studies on the non-prompt and fake lepton composition. This sample is simulated with `PYTHIA` v8 [40] and includes all the relevant $2 \to 2$ QCD processes, filtered at truth level to mimic a level-1 electromagnetic trigger requirement.

All `PYTHIA6` samples use `PHOTOS` v2.15 [41] to simulate photon radiation and `TAUOLA` v1.20 [42] to simulate τ decays. The simulated events are weighted such that the distribution of the average number of pp interactions per bunch crossing agrees with data. All samples are processed through a simulation [43] of the detector geometry and response using `GEANT4` [44]. Table 1 provides a summary of the MC samples used in the analysis. All simulated samples are processed through the same reconstruction software as the data.

To improve the W/Z+jets background modeling, the simulated W/Z p_{T} spectrum is reweighted to match the one reconstructed in data. In addition the yields of $ZQ\bar{Q}(Q = b, c)$ are also corrected to match the observed one (see Ref. [6]).

4 Object reconstruction

Electron candidates [45] are reconstructed from isolated electromagnetic calorimeter energy deposits matched to inner detector tracks and passing identification requirements, with transverse energy E_{T}> 25 GeV and pseudorapidity $|\eta_{\mathrm{cluster}}|$ <2.47 (where η_{cluster} is the pseudorapidity of the calorimeter cluster associated with the electron candidate). Those within the transition region between the barrel and end-cap electromagnetic calorimeters, $1.37 < |\eta_{\mathrm{cluster}}| < 1.52$, are removed. Isolation requirements are used to reduce backgrounds from non-prompt and fake electrons, by applying cuts on the calorimeter transverse energy within a cone of size $\Delta R = \sqrt{(\Delta\eta)^2 + (\Delta\phi)^2} < 0.2$ and the scalar sum of track transverse momentum p_{T} within $\Delta R < 0.3$, in each case excluding the contribution from the electron itself. These two quantities are each required to be smaller than E_{T} and η-dependent thresholds calibrated to separately give nominal selection efficiencies of 90% for prompt electrons from $Z \to ee$ decays. Electron candidates passing tight [45] selection criteria and the isolation requirements are referred to as tight electrons. Loose electrons are electrons satisfying tight [45] selection criteria but where the requirements on TRT-based particle identification and on the energy-to-momentum ratio E/p are relaxed and no requests on the isolation are made.

Muon candidates are reconstructed by combining matching tracks reconstructed in both the inner detector and muon spectrometer [46], and required to satisfy p_{T}>25 GeV and $|\eta|$ <2.5. Isolation requirements are also introduced, asking for $I < 0.05$, where I is the ratio of the sum of track p_{T} in a variable-sized cone of radius $\Delta R = 10\ \mathrm{GeV}/p_{\mathrm{T}}^{\mu}$ to the transverse momentum p_{T} of the muon. These muons are referred to as 'tight muons'. For loose muons, no request on the isolation is made but all other selection requirements are applied.

The probability that a lepton from a W/Z decay (non-prompt or fake lepton) identified as a loose lepton satisfies the tight identification criteria is defined 'real efficiency' ε_{r}, and 'fake efficiency' as ε_{f}

respectively.

Jets are reconstructed with the anti-k_t algorithm [47,48] with radius parameter $R = 0.4$, starting from calorimeter energy clusters calibrated using the local cluster weighting method [49]. Jets are calibrated using an energy- and η-dependent simulation-based calibration scheme, with in-situ corrections based on data, and are required to satisfy p_{T}>25 GeV and $|\eta|$ <2.5. To suppress the contribution from low-p_{T} jets originating from pileup interactions, a validation based on tracks that the jet comes from the primary vertex is applied to jets with p_{T}<50 GeV and $|\eta|$ <2.4: jets are required to have at least 50% of the scalar sum of the p_{T} of tracks associated to the jet coming from tracks associated to the event primary vertex. The primary vertex is defined as the reconstructed vertex with the highest sum of associated track p_{T}^2.

During jet reconstruction, no distinction is made between identified electrons and jet energy deposits. Therefore, if any of the jets lie within $\Delta R < 0.2$ of a selected electron, the closest jet is discarded in order to avoid double-counting of electrons as jets. Finally, to further suppress non-isolated leptons from heavy-flavour decays inside jets, electrons and muons within $\Delta R < 0.4$ of selected jets are also discarded. This procedure is repeated separately for the loose and tight leptons.

Jets are identified as containing a b-quark (b-tagged) via an algorithm [50] using multivariate techniques to combine information from the impact parameters of displaced tracks as well as topological properties of secondary and tertiary decay vertices reconstructed within the jet. The working point used for this measurement corresponds to 70% efficiency to tag a b-quark jet, with a light-jet rejection factor of ∼130 and a charm jet rejection factor of 5, as determined for b-tagged jets with p_{T}>20 GeV and $|\eta|$ <2.5 in simulated $t\bar{t}$ events. The efficiency of the the b-tagging algorithm is measured for each jet flavour using control samples in data and compared to the simulation. In the case of b-jets, scale factors are estimated based on observed and simulated b-tagging rates in $t\bar{t}$ events [51]. In the case of c-jets, they are derived based on jets with identified D mesons [52]. In the case of light-flavour jets, scale factors are derived using dijet event [53].

The missing transverse energy is reconstructed from the vector sum of all calorimeter cell energies associated with topological clusters with $|\eta|$ <4.5 [54]. Contributions from the calorimeter clusters matched with either a reconstructed lepton or jet are corrected to the corresponding energy scale. The term accounting for the selected muon p_{T} is included into the calculation. The symbol $E_{\mathrm{T}}^{\mathrm{miss}}$ is used for its magnitude.

5 Event selection

Events are required to pass either a single electron or single muon trigger. The p_{T} thresholds are 24 or 60 GeV for electrons (labelled e24vhi and e60) and 24 or 36 GeV for muons (labelled mu24i and mu36). The triggers with the lower p_{T} threshold include isolation requirements on the candidate lepton that are looser than those applied for the identification of tight leptons. Additional pre-scaled triggers without isolation requirements (e24vh and mu24) are considered in the following, but are not used to select events unless specified.

The events selected to study top quark pair and single top production in the lepton+jets and dilepton channels have one or two leptons (electrons or muons), a significant amount of missing transverse energy and a number of jets and b-jets In the lepton+jets channels (e+jets and μ+jets), the presence of exactly one loose or tight electron or muon is required. In the following, when not specified, a tight lepton is required. To suppress the non-prompt and fake lepton backgrounds, besides the cut in $E_{\mathrm{T}}^{\mathrm{miss}}$, a cut on the transverse mass of the lepton and $E_{\mathrm{T}}^{\mathrm{miss}}$ can be introduced. It is defined as $m_{\mathrm{T}}^{\mathrm{W}} = \sqrt{2p_{\mathrm{T}}^{\mathrm{lepton}} E_{\mathrm{T}}^{\mathrm{miss}}(1-\cos\Delta\phi)}$, where $\Delta\phi$ is the difference in azimuthal angle between the lepton and $E_{\mathrm{T}}^{\mathrm{miss}}$. The dileptonic event selection typically requires the presence of two opposite-sign charge (OS) leptons, and, in case of the $e\mu$ channel (which is the only dilepton channel where results are pre-

sented here) a cut on the sum of the p_{T} of leptons and jets in the event, a quantity referred to as H_{T} in the following. Details of the $t\bar{t}$ semileptonic and dileptonic event selections can be found in Ref. [55]. In what follows, if the quality of the leptons is not specified, the two leptons are required to be tight.

Table 2: Summary of the signal regions considered in the analysis. The term 'pretag' is used to indicate that no requirements on the number of b-jets are applied, while 'OS' stands for opposite sign charged leptons.

Channel	n_{jet} / $n_{b-\mathrm{jet}}$ cuts	Other cuts
e+jets	2 jets, pretag 2 jets, ≥ 1 b-tags $\geq$4 jets, pretag $\geq$4 jets, ≥ 1 b-tags	$E_{\mathrm{T}}^{\mathrm{miss}}$>30 GeV, $m_{\mathrm{T}}^{\mathrm{W}}$>30 GeV
μ+jets	2 jets, pretag 2 jets, ≥ 1 b-tags $\geq$4 jets, pretag $\geq$4 jets, ≥ 1 b-tags	$E_{\mathrm{T}}^{\mathrm{miss}}$>20 GeV, $E_{\mathrm{T}}^{\mathrm{miss}}+m_{\mathrm{T}}^{\mathrm{W}}$>60 GeV
$e\mu$	$\geq$2 jets, pretag $\geq$2 jets, ≥ 1 b-tags	OS, $H_{\mathrm{T}} > 100$ GeV

In the presented analysis, for each of the considered lepton+jets or dilepton channels, different signal regions are defined by the requirements summarised in Table 2. These are typical regions where the $t\bar{t}$ signal is extracted, or, in case of the two-jet regions, the dominant real lepton background from W+jets is controlled. Here and in the following, the term 'pretag' is used to refer to a region without any requirement on the number of b-jets, *i.e* events with 0, 1 or at least 2 b-jets.

6 Matrix method

6.1 Overview

In a data sample containing events with a single lepton, the number of events with one tight lepton (N^{t}) and the number of events with one loose lepton (N^{l}) can be expressed as linear combinations of the number of events with a real or a non-prompt or fake lepton:

$$\begin{aligned} N^{\mathrm{l}} &= N_{\mathrm{r}}^{\mathrm{l}} + N_{\mathrm{f}}^{\mathrm{l}}, \\ N^{\mathrm{t}} &= \varepsilon_{\mathrm{r}}\, N_{\mathrm{r}}^{\mathrm{l}} + \varepsilon_{\mathrm{f}}\, N_{\mathrm{f}}^{\mathrm{l}}, \end{aligned} \tag{1}$$

where ε_{r} is the fraction of real leptons in the loose selection that also pass the tight one and ε_{f} is the fraction of non-prompt and fake lepton backgrounds in the loose selection that also pass the tight selection.

If ε_{r} and ε_{f} are known, the number of events with a non-prompt or fake lepton can be calculated from Eq. 1 given the measured N^{l} and N^{t}. The relative efficiencies ε_{r} and ε_{f} are measured in data in control samples enriched in either real or non-prompt or fake lepton. The number of tight events coming from non-prompt or fake lepton backgrounds can be expressed as:

$$N_{\mathrm{f}}^{\mathrm{t}} = \frac{\varepsilon_{\mathrm{f}}}{\varepsilon_{\mathrm{r}} - \varepsilon_{\mathrm{f}}} (\varepsilon_{\mathrm{r}}\, N^{\mathrm{l}} - N^{\mathrm{t}}). \tag{2}$$

The matrix method efficiencies ε_{r} and ε_{f} depend on lepton kinematics and event characteristics, such as and the number of jets or b-jets. To correctly account for this, an event weight is computed

from the efficiencies, which are parametrised as a function of the various object kinematics (as detailed Section 6.2):

$$w_i = \frac{\varepsilon_{\mathrm{f}}}{\varepsilon_{\mathrm{r}} - \varepsilon_{\mathrm{f}}} (\varepsilon_{\mathrm{r}} - \delta_{\mathrm{i}}), \tag{3}$$

where δ_{i} equals unity if the loose event i passes the tight event selection and 0 otherwise. The background estimate in a given bin of the final observable is given by the sum of w_i over all events in that bin.

In the case of a dilepton selection, the numbers of observed events with two tight leptons (denoted as N_{tt}), one loose and one tight lepton (N_{tl} and N_{lt}) or two loose leptons (N_{ll}) are counted. Here and in what follows, the leptons are ordered by p_{T} in the indexes, such that the leading lepton in N_{tl} region is tight and the leading lepton in N_{lt} is loose. Using ε_{r} and ε_{f}, already defined for the single lepton case, linear equations are obtained for the observed yields as a function on the number of events with zero, one and two real leptons together with two, one and zero non-prompt or fake leptons (N_{ff}, N_{rf}, N_{fr} and N_{fr} respectively):

$$\begin{pmatrix} N_{\mathrm{rr}} \\ N_{\mathrm{fr}} \\ N_{\mathrm{rf}} \\ N_{\mathrm{ff}} \end{pmatrix} = \mathbf{M^{-1}} \begin{pmatrix} N_{\mathrm{tt}} \\ N_{\mathrm{tl}} \\ N_{\mathrm{lt}} \\ N_{\mathrm{ll}} \end{pmatrix}, \tag{4}$$

where $\mathbf{M}$ is a 4×4 matrix written in terms of ε_{r} and ε_{f}. It is calculated as:

$$\mathbf{M} = \begin{pmatrix} \varepsilon_{r,1}\,\varepsilon_{r,2} & \varepsilon_{r,1}\,\varepsilon_{\mathrm{f},2} & \varepsilon_{\mathrm{f},1}\,\varepsilon_{r,2} & \varepsilon_{\mathrm{f},1}\,\varepsilon_{\mathrm{f},2} \\ \varepsilon_{r,1}\,\overline{\varepsilon_{r,2}} & \varepsilon_{r,1}\,\overline{\varepsilon_{\mathrm{f},2}} & \varepsilon_{\mathrm{f},1}\,\overline{\varepsilon_{r,2}} & \varepsilon_{\mathrm{f},1}\,\overline{\varepsilon_{\mathrm{f},2}} \\ \overline{\varepsilon_{r,1}}\,\varepsilon_{r,2} & \overline{\varepsilon_{r,1}}\,\varepsilon_{\mathrm{f},2} & \overline{\varepsilon_{\mathrm{f},1}}\,\varepsilon_{r,2} & \overline{\varepsilon_{\mathrm{f},1}}\,\varepsilon_{\mathrm{f},2} \\ \overline{\varepsilon_{r,1}}\,\overline{\varepsilon_{r,2}} & \overline{\varepsilon_{r,1}}\,\overline{\varepsilon_{\mathrm{f},2}} & \overline{\varepsilon_{\mathrm{f},1}}\,\overline{\varepsilon_{r,2}} & \overline{\varepsilon_{\mathrm{f},1}}\,\overline{\varepsilon_{\mathrm{f},2}} \end{pmatrix}, \tag{5}$$

where the index on ε_{r} and ε_{f} refers to the first (1) or second (2) lepton in the event, and $\bar{\varepsilon}$ stands for $(1 - \varepsilon)$. Similarly to the single lepton case, four weights, w_{rr}, w_{rf}, w_{fr} and w_{ff} are calculated on event-by-event basis. The probability that an event with two loose leptons contains at least one non-prompt or fake lepton is then given by $w_{\mathrm{rf}} + w_{\mathrm{fr}} + w_{\mathrm{ff}}$. Finally, the estimated background contribution in a sample of events with two tight leptons is given by the event weight:

$$w_{\mathrm{tt}} \quad = \quad \varepsilon_{r,1}\,\varepsilon_{\mathrm{f},2}\,w_{\mathrm{rf}} + \varepsilon_{\mathrm{f},1}\,\varepsilon_{r,2}\,w_{\mathrm{fr}} + \varepsilon_{\mathrm{f},1}\,\varepsilon_{\mathrm{f},2}\,w_{\mathrm{ff}}\ . \tag{6}$$

6.2 Measurement and parametrisation of the efficiencies

Real and fake efficiencies ε_{r} and ε_{f} are measured in control regions which are representative of the signal regions in terms of kinematics and, in the case of the fake efficiency, non-prompt and fake lepton background composition. Table 3 summarises the definition of the different control regions used to extract the real and fake efficiencies, as explained in the following.

The real efficiencies ε_{r} are measured using the tag-and-probe method from the $Z\rightarrow ee$ and $Z\rightarrow \mu\mu$ control regions. This method selects an unbiased sample of loose leptons (probes) from the Z boson decay by using a tight selection requirement on the other object produced from the particle's decay (tags). The efficiency is determined by applying the tight selection to the probe lepton. For each pair, the tag and the probe leptons are required to have opposite reconstructed charges. A typical dilepton invariant mass range used in this analysis is 80 to 100 GeV, although this range is varied in systematic studies. After this selection, the sample still contains non-prompt and fake lepton backgrounds. The background is determined using a side band subtraction approach and is found to be at the percent level. In the case of electrons, for which the identification is more sensitive to jet activity in the event, ε_{r} is corrected to match the expected efficiency in $t\bar{t}$ events. The correction is calculated from comparisons of

Table 3: Summary of the different control regions used to extract the matrix method efficiencies. The term 'pretag' is used to indicate that no requirements on the number of b-jets are applied, while 'OS' stays for opposite-sign charge leptons.

Channel	n_{jet} / $n_{b-\text{jet}}$ cuts	Other cuts	Used for
e+jets	≥1 jets, pretag	m_{T}^{W}<20 GeV, $E_{\text{T}}^{\text{miss}}+m_{\text{T}}^{\text{W}}$<60 GeV	$\varepsilon_{\text{f}}(e)$ extraction
μ+jets	≥1 jets, pretag	$\lvert d_0^{\text{sig}}\rvert > 5$	$\varepsilon_{\text{f}}(\mu)$ extraction
ee	≥1 jets, pretag	OS, 80 GeV < m_{ee} < 100 GeV	$\varepsilon_{\text{r}}(e)$ extraction
$\mu\mu$	≥1 jets, pretag	OS, 80 GeV < $m_{\mu\mu}$ < 100 GeV	$\varepsilon_{\text{r}}(\mu)$ extraction

values determined in $t\bar{t}$ and Z simulated events. This correction is derived separately for each of the bins where ε_{r} is measured (see later in the text) and is on average -3%.

The fake efficiencies ε_{f} are measured in data samples dominated by non-prompt and fake lepton background events. These control regions, denoted CR_{f}, contain only one loose lepton, at least one jet and have low $E_{\text{T}}^{\text{miss}}$ and/or m_{T}^{W} or high lepton impact parameter. Distributions of the variables used to define CR_{f} are shown in Fig. 1. For e+jets events CR_{f} is defined by $m_{\text{T}}^{\text{W}} < 20$ GeV & $m_{\text{T}}^{\text{W}} + E_{\text{T}}^{\text{miss}} < 60$ GeV. For μ+jets events CR_{f} is defined by $|d_0^{\text{sig}}| > 5$, where d_0^{sig} is the muon impact parameter significance, $d_0^{\text{sig}} = d_0/\sqrt{err(d_0)}$. In the case of muons, a linear extrapolation of the dependence on d_0^{sig} from CR_{f} to the inclusive selection is performed. The result of this extrapolation is an overall increase of up to 5%, depending on the number of b-jets and the trigger (see later). The contribution from processes containing prompt leptons, such as Z+jets, W+jets, $t\bar{t}$, single top and diboson, are determined using MC simulation. In events with one tight electron (muon), the contamination from these processes is of order 50% (15%). Efficiencies are determined as the ratio between the number of tight and loose events in these regions.

One of the two triggers used to select events has an isolation requirement, while loose leptons are defined without any isolation cut. Efficiencies are therefore expected to be different for leptons matched to the trigger with or without isolation. Efficiencies are thus derived and applied depending on the trigger being fired by the lepton (see section 5) and on the lepton p_{T} being below or above the high-p_{T} trigger threshold. Efficiencies extracted in the case of the e24vh (mu24) trigger are used in the dilepton channel for electrons (muons) below the high-p_{T} trigger threshold not matched to the e24vhi (mu24i) trigger.

Beside the dependence on the fired trigger described above, the values of ε_{r} and ε_{f} are measured as a function of different variables, including: the lepton $|\eta|$ and p_{T}, the angular distance between the lepton and the closest jet (min $\Delta R(\ell, \text{jet})$), the angle in the transverse plane between the lepton and the $E_{\text{T}}^{\text{miss}}$ ($\Delta\phi(\ell, \text{E}_{\text{T}}^{\text{miss}})$), the p_{T} of the leading jet, the jet and b-jet multiplicity in the event. Fig. 2 and 3 show ε_{r} and ε_{f}, as a function of the different variables used for the parametrisation. Efficiencies are shown inclusively for electrons and muons in events with at least one jet and any number of b-jets, but separately for leptons firing each of the triggers, and in the relative lepton p_{T} regions. The significant dependency of the muon real and fake efficiencies on the muon p_{T} originates from the isolation requirements imposed to define a tight muon.

These efficiencies are used to compute the weights in Eq. 3 as a function of the different combinations of the variables listed above through:

$$\varepsilon_k(x_1, ..., x_N; y_1, ..., y_M) = \frac{1}{\varepsilon_k(x_1, ..., x_N)^{M-1}} \cdot \prod_{j=1}^{M} \varepsilon_k(x_1, ..., x_N; y_j). \tag{7}$$

Here the expression $\varepsilon_k(x_1, ..., x_N)$ represents the efficiency measured as a function of all the x variables. The expresssion $\varepsilon_k(x_1, ..., x_N; y_j)$ represents instead the efficiency measured as a function of all the x variables and of the variable y_j. Equation 7 implies that the full correlation between the variables x (typ-

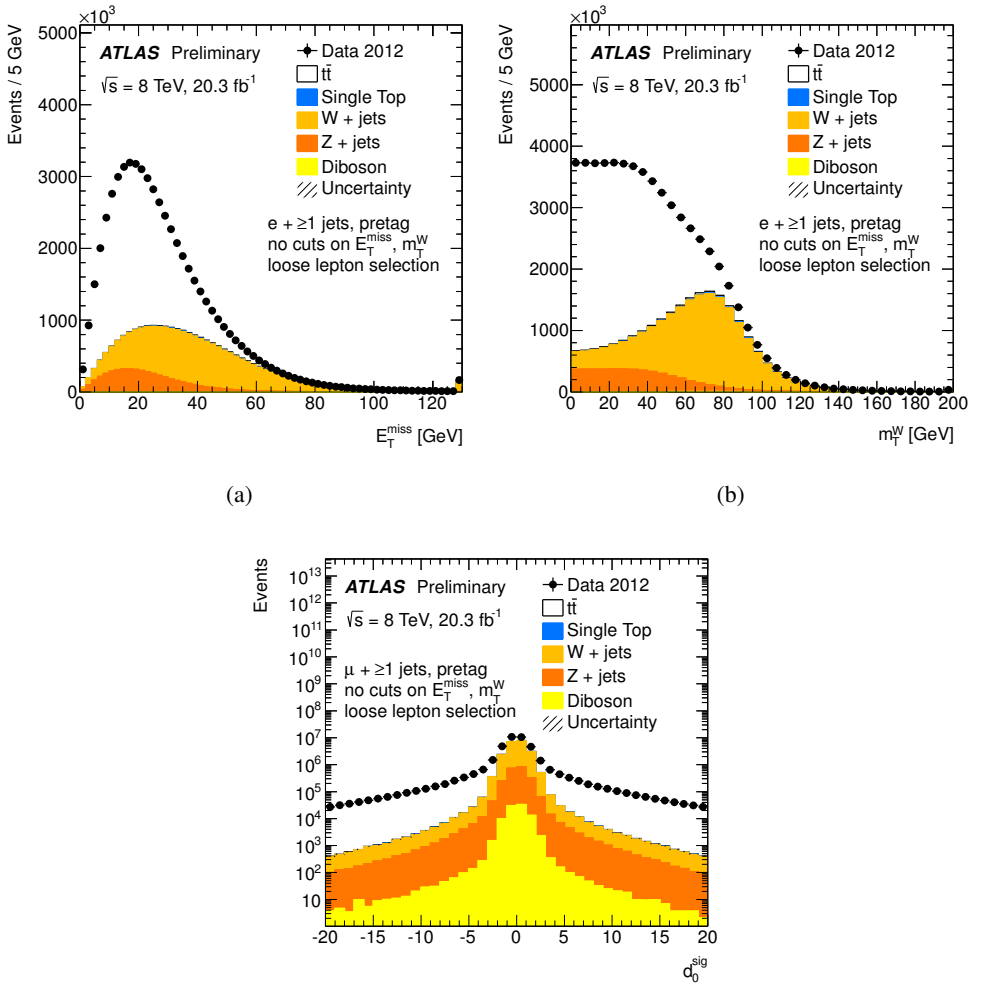

Figure 1: Distributions of the $E_{\mathrm{T}}^{\mathrm{miss}}$ (a) and $m_{\mathrm{T}}^{\mathrm{W}}$ (b) in e+jets events and the transverse impact parameter significance d_0^{sig} (c) in μ+jets events for data and real lepton expectation from simulated events. Events are required to have exactly one loose electron or muon and at elast one jet, with no requests on the number of b-tags and no cuts on $E_{\mathrm{T}}^{\mathrm{miss}}$ or $m_{\mathrm{T}}^{\mathrm{W}}$. The region between the top of the stacked simulated sources and the data is assumed to come from the non-prompt and fake lepton background contribution. The only uncertainty shown is the statistical one due to finite Monte Carlo event samples.

ically discrete variables, where no more than three bins are used) and each of the variables y (typically continuous variables, with a relatively large number of bins) is taken into account, while the correlation between the y variables is neglected. For each of the efficiencies ε_k, only a sub-set of the variables in each category, x or y, is used, as summarised in Table 4. This choice is driven by the observed dependencies, the correlations between the variables and the stability of the estimates. In particular, for each of the efficiencies, the assumption of no correlation between the variables y is checked by comparing the observed dependency on the variable y_j, *i.e.* $\varepsilon_k(x_1, ..., x_N; y_j)$, and the efficiency $\varepsilon_k(x_1, ..., x_N; y_1, ...y_M)$ averaged over all the other $\{y_{j'}\}_{j' \neq j}$ variables.

The main sources of systematic uncertainties on the non-prompt and fake lepton background determination with the matrix method originate from the determination of the real efficiency, the use of MC

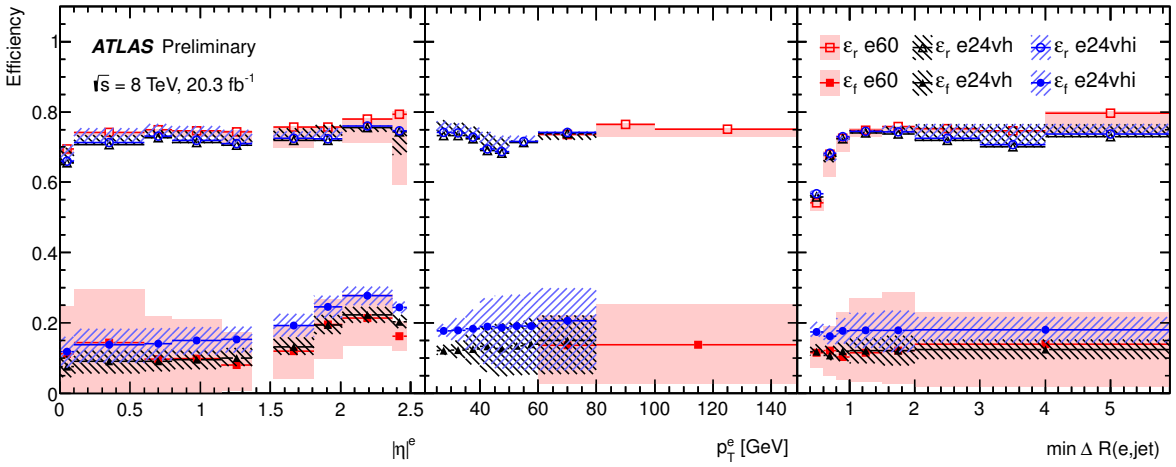

(a)

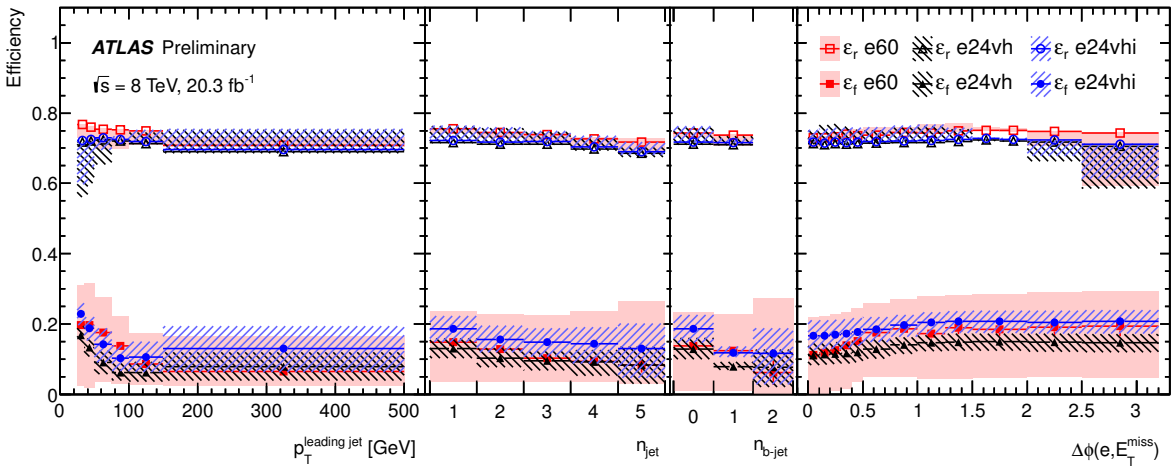

(b)

Figure 2: Efficiencies ε_{r} and ε_{f} for electrons, as measured in data (see text for details), as a function of (from left to right): (a) the electron $|\eta|$ and p_{T} its distance to the closest jet (min $\Delta R(\mathrm{e},\mathrm{jet})$), (b) the p_{T} of the leading jet, the jet and b-jet multiplicity and the angle in the transverse plane between the electron and the $E_{\mathrm{T}}^{\mathrm{miss}}$ ($\Delta\phi(\mathrm{e},\mathrm{E}_{\mathrm{T}}^{\mathrm{miss}})$). The efficiencies are shown separately for probes which match specifically one of the triggers used to selected data (e24vhi or e60) or the low-p_{T} trigger with no isolation requirement (e24vh). The shaded area represents in each bin the combination of the statistical and systematic uncertainties on the efficiency measurements. The systematic uncertainties include the effect of using the alternative control regions (for both ε_{r} and ε_{f}), and the variations on the amount of real lepton events (for ε_{f}).

simulation to correct the efficiency measurements, differences in the non-prompt and fake background composition in the signal regions and in the regions used to measure the efficiencies, and the treatment of the dependence of the efficiencies on lepton and event properties.

The uncertainty on the real efficiency measurement method is assessed by measuring the efficiency in an independent way, by counting the fraction of tight leptons after selecting events with one loose electron

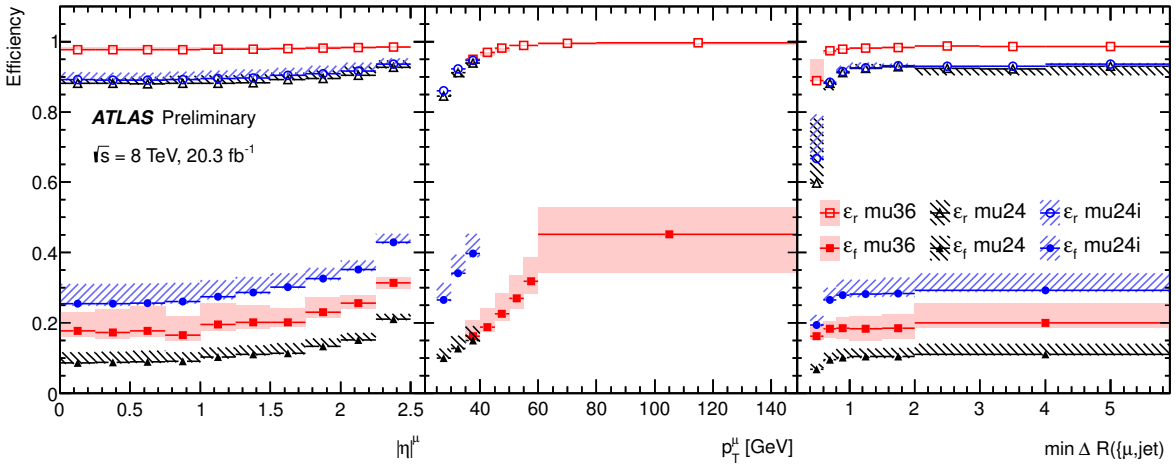

(a)

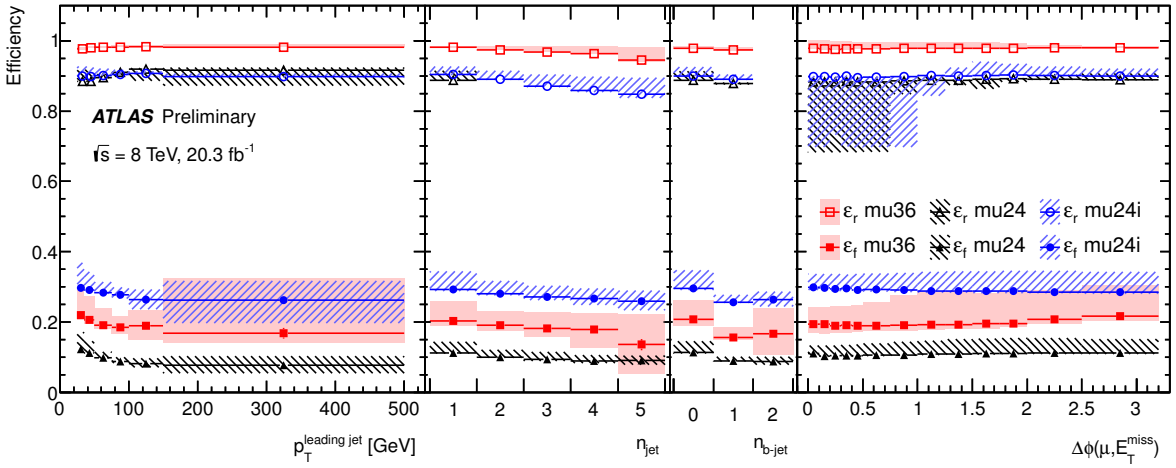

(b)

Figure 3: Efficiencies ε_{r} and ε_{f} for muons, as measured in data (see text for details), as a function of (from left to right): (a) the muon $|\eta|$ and p_{T} its distance to the closest jet (min $\Delta R(\mu, \mathrm{jet})$), (b) the p_{T} of the leading jet, the jet and b-jet multiplicity and the angle in the transverse plane between the muon and the $E_{\mathrm{T}}^{\mathrm{miss}}$ ($\Delta\phi(\mu, \mathrm{E}_{\mathrm{T}}^{\mathrm{miss}})$). The efficiencies are shown separately for probes which match specifically one of the triggers used to selected data (mu24i or mu36) or the low-p_{T} trigger with no isolation requirement (mu24). The shaded area represents the combination in each bin of the statistical and systematic uncertainties on the efficiency measurements. The systematic uncertainties include the effect of using the alternative control regions (for both ε_{r} and ε_{f}), and the variations on the amount of real lepton events (for ε_{f}).

(muon) in a regions where the contamination from non-prompt and fake lepton events is expected to be negligible, *i.e.* by asking $E_{\mathrm{T}}^{\mathrm{miss}} > 150$ GeV ($m_{\mathrm{T}}^{\mathrm{W}} > 100$ GeV). It is found to be around 7% (between 1 and 5%) in the case of electrons (muons) and to be comparable to the uncertainties on the measurement using the tag-and-probe method. The latter uncertainties, found to be around 3% for electrons and between 1 and 2% for muons, are dominated by the modeling of the background and the uncertainty on the

Table 4: Summary of the variables used to parametrise the real and fake lepton efficiencies in the matrix method. The column 'Trigger' refers to the specific trigger the lepton matches, $p_{\mathrm{T}}^{\mathrm{lead.jet}}$ stays for p_{T} of the leading jet in the event, $\Delta R(\ell, \mathrm{jet})$ is the angular distance between the lepton and the closest jets, $\Delta\phi(\ell, \mathrm{E}_{\mathrm{T}}^{\mathrm{miss}})$ is the angular distance in the transverse plane between the lepton and the missing energy in the event. For each of the efficencies, the variables for which the explicit dependence is used are indicated. The variables are divided in two categories, x and y, depending the specifc treatment in terms of correlation. See text for details.

	x variables			y variables				
	Trigger	n_{jet}	$n_{b-\mathrm{jet}}$	$\lvert\eta^{\ell}\rvert$	p_{T}^{ℓ}	$p_{\mathrm{T}}^{\mathrm{lead.jet}}$	$\Delta R(\ell, \mathrm{jet})$	$\Delta\phi(\ell, \mathrm{E}_{\mathrm{T}}^{\mathrm{miss}})$
$\varepsilon_{\mathrm{r}}(e)$	✓	✓		✓	✓		✓	
$\varepsilon_{\mathrm{r}}(\mu)$	✓	✓		✓	✓		✓	
$\varepsilon_{\mathrm{f}}(e)$	✓		✓	✓		✓		✓
$\varepsilon_{\mathrm{f}}(\mu)$	✓		✓	✓	✓		✓	

correction based on MC simulation applied in the case of electrons.

The dominant source of systematic uncertainty on the fake efficiency measurement is that originating from the uncertainty on the normalisation of the processes determined from MC simulation in the control regions (mainly Z+jets and W+jets). The uncertainty of their normalisation is ~30% and corresponds to an uncertainty of 3-13% on the fake efficiency. Another significant source of uncertainty is assessed through the use of alternative control regions to measure the efficiencies, defined by different combinations of cuts on $E_{\mathrm{T}}^{\mathrm{miss}}$ and $m_{\mathrm{T}}^{\mathrm{W}}$, *i.e.* $m_{\mathrm{T}}^{\mathrm{W}} < 20$ GeV for e+jet, $m_{\mathrm{T}}^{\mathrm{W}} < 20$ GeV and $E_{\mathrm{T}}^{\mathrm{miss}} + m_{\mathrm{T}}^{\mathrm{W}} < 60$ GeV for μ+jet events. This approach allows to partially assess the uncertainty coming from the relative composition of the non-prompt and fake lepton samples in the control and signal regions. Preliminary studies, performed in the case of electrons using simulated events, indicate that this relative composition changes between the control and the single lepton signal regions by the same amount as it does between the default and the alternative control regions. The uncertainty is found to be between 2 and 5%, comparable to the one found in comparing the fake rates measured in data samples enriched in electrons from conversions, semi-leptonic decays of b/c quarks or hadrons (between 5 and 7%). No dedicated systematic uncertainty is applied to the d_0^{sig} extrapolation used for muon ε_{f}: the effect of applying or not the correction is already covered by the other systematic uncertainties, in particular the variation on the amount of real lepton events, which modifies significantly the slope of the linear extrapolation, and the use of the alternative $\mathrm{CR_f}$, for which no extrapolation is performed.

Finally, different choices for the combinations of variables used in the efficiency parametrisation are compared. In particular, the most relevant variations are found to come from the use of min $\Delta R(\mathrm{e}, \mathrm{jet})$ instead of $\Delta\phi(\mathrm{e}, \mathrm{E}_{\mathrm{T}}^{\mathrm{miss}})$ in the electron ε_{f} parametrisation and $p_{\mathrm{T}}^{\mathrm{leading\,jet}}$ instead of p_{T}^{μ} in the muon ε_{f} one, and are used to assess the uncertainty related to the treatment of the efficiency dependencies on lepton and event properties.

To evaluate the uncertainty on the non-prompt and fake and background contribution, the matrix method input efficiencies are varied as described above, and the background distributions and yields are then re-derived. The observed deviation of the yields measured where lepton efficiencies are varied is assigned as an uncertainty. The total systematic uncertainty on the estimate is taken as the quadratic sum of the symmetrised individual variations.

In the single-lepton signal regions, this is between 10 and 50%, depending on the channel and on the jet and b-jet multiplicity. The use of the alternative parametrisation and the real lepton subtraction from $\mathrm{CR_f}$ are the dominant sources, with effects between 20 and 40% each, in the e+jets channel. In the μ+jets channel, beside these two sources of uncertainties, with effects between 10 and 25%, the

Table 5: Summary of the different validation regions used for the matrix method. The term 'pretag' is used to indicate that no requirements on the number of b-jets are applied, '!tt' refers to a selection where at least one of the two leptons is not tight, 'OS' stays for opposite-sign and 'SS' for same-sign charge leptons.

Channel	n_{jet} / $n_{b-\text{jet}}$ cuts	Other cuts
e+jets	2 jets, pretag 2 jets, ≥ 1 b-tags $\geq$4 jets, pretag $\geq$4 jets, ≥ 1 b-tags	No cuts on $E_{\text{T}}^{\text{miss}}$, m_{T}^{W}
μ+jets	2 jets, pretag 2 jets, ≥ 1 b-tags $\geq$4 jets, pretag $\geq$4 jets, ≥ 1 b-tags	No cuts on $E_{\text{T}}^{\text{miss}}$, m_{T}^{W}
$e\mu$	$\geq$2 jets, pretag $\geq$2 jets, ≥ 1 b-tags	SS, $H_{\text{T}} > 100$ GeV
	$\geq$2 jets, pretag $\geq$2 jets, ≥ 1 b-tags	OS, !tt, $H_{\text{T}} > 100$ GeV

alternative estimate for ε_{r} produces a relatively large deviation, around 15%.

6.3 Results in lepton+jets validation regions as obtained using the matrix method

The background predictions are compared to data in validation regions, summarised in Table 5. In the lepton+jets channels, these regions are defined as the signal regions but without applying the $E_{\text{T}}^{\text{miss}}$ and m_{T}^{W} cuts. These regions include the control regions where the fake efficiencies are measured and are therefore used to carry out a consistency check of the method.

Fig. 4 shows the distributions of $E_{\text{T}}^{\text{miss}}$ and m_{T}^{W} in the e+jets validation regions with two jets. Distributions show the non-prompt and fake lepton background estimates together with the real lepton predictions from MC simulation and compared with data. Similarly, Fig. 5 shows the same distributions for μ+jets events. In Appendix B results in regions with four or more jets are shown. The agreement between data and prediction is within the uncertainty of the non-prompt and fake background in regions of phase space where this background dominates. In regions where it is negligible, data and prediction agree within the uncertainties on the MC-derived processes based on Ref. [56]. Note that the uncertainty band shown in the Figures does not contain the uncertainty on the MC-derived backgrounds.

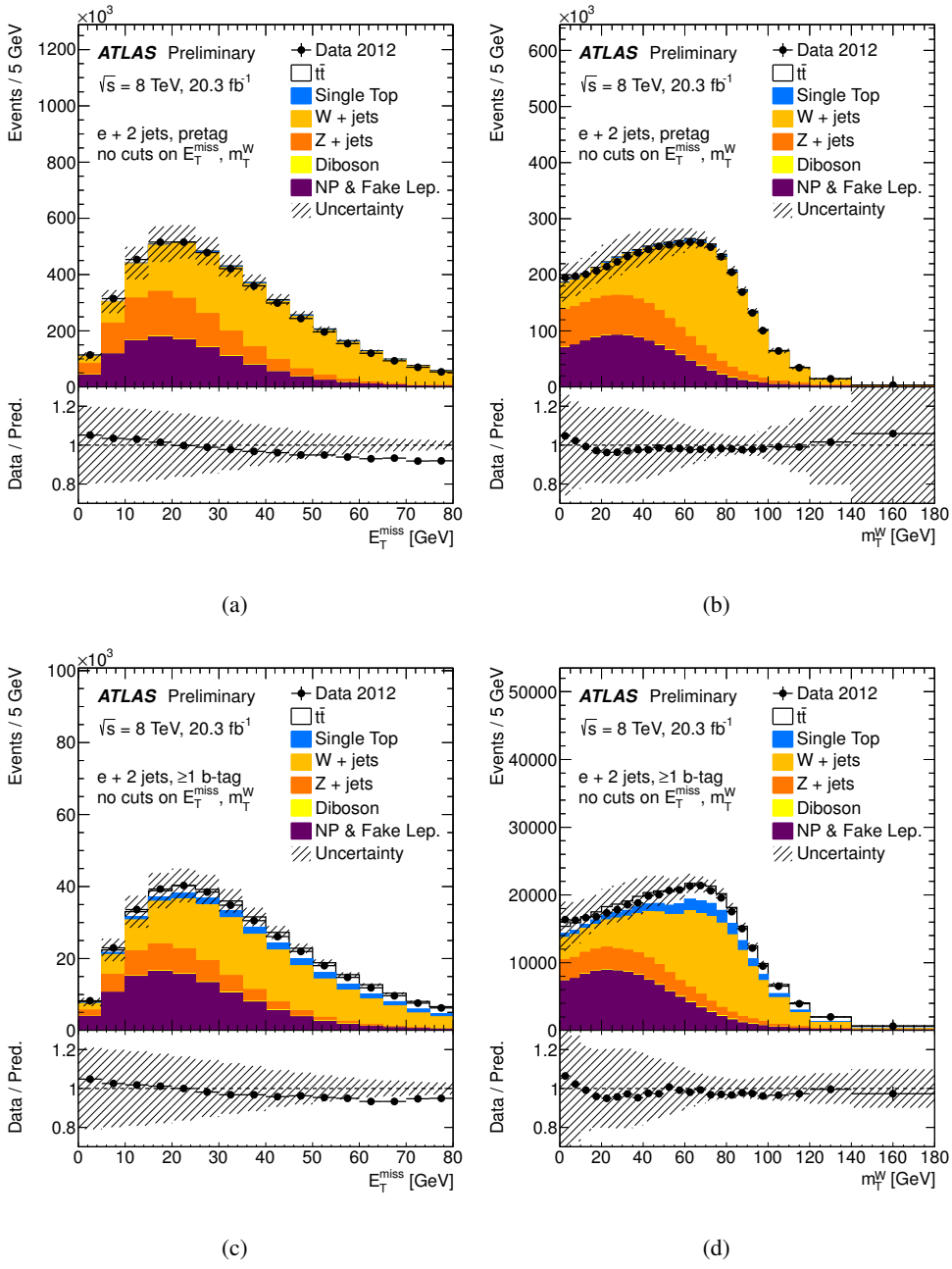

Figure 4: Distributions of $E_{\mathrm{T}}^{\mathrm{miss}}$ (a, c) and $m_{\mathrm{T}}^{\mathrm{W}}$ (b, d) in e+jets events with exactly two jets before (a, b) and after (c, d) requiring at least one b-jet, without any cuts on $E_{\mathrm{T}}^{\mathrm{miss}}$ and $m_{\mathrm{T}}^{\mathrm{W}}$. The data is compared to the real lepton expectation from simulation, showing separately the contributions from $t\bar{t}$, single top, W+jets, Z+jets and dibosons normalised to their cross-sections, and non-prompt and fake lepton backgrounds (referred to as 'NP & Fake Lep.') estimated with the matrix method. The shaded area represents the combination of the statistical and the systematic uncertainties on the matrix method estimate in each bin. The systematic uncertainties on the processes predicted by the MC simulation are not shown.

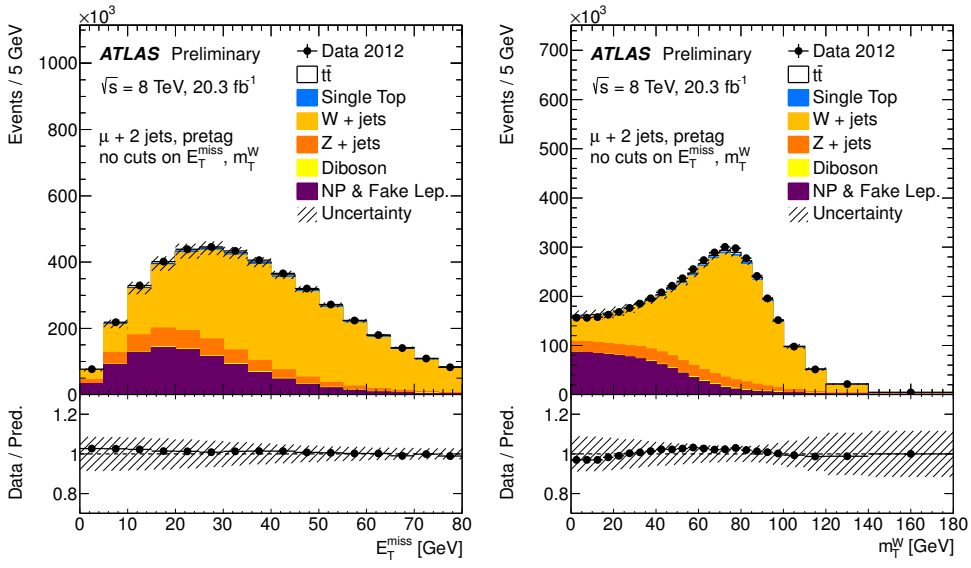

(a) (b)

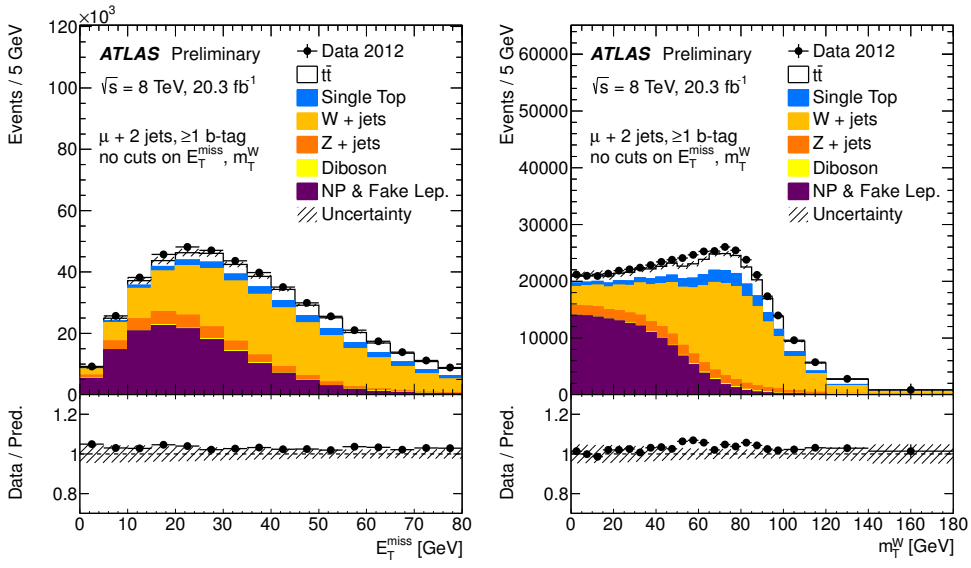

(c) (d)

Figure 5: Distributions of $E_{\mathrm{T}}^{\mathrm{miss}}$ (a, c) and $m_{\mathrm{T}}^{\mathrm{W}}$ (b, d) in μ+jets events with exactly two jets before (a, b) and after (c, d) requiring at least one b-jet, without any cuts on $E_{\mathrm{T}}^{\mathrm{miss}}$ and $m_{\mathrm{T}}^{\mathrm{W}}$. The data is compared to the real lepton expectation from simulation, showing separately the contributions from $t\bar{t}$, single top, W+jets, Z+jets and dibosons normalised to their cross-sections, and non-prompt and fake lepton backgrounds (referred to as 'NP & Fake Lep.') estimated with the matrix method. The shaded area represents the combination of the statistical and the systematic uncertainties on the matrix method estimate in each bin. The systematic uncertainties on the processes predicted by the MC simulation are not shown.

6.4 Results in $t\bar{t}$ dilepton events as obtained using the matrix method

For the dilepton case, besides the signal regions introduced in Table 2, the validation regions are defined by the presence of two same-sign (SS) leptons, or by the presence of at least one non-tight lepton (!tt), as reported in Table 5. Note that, in contrast to the lepton+jet case, these validation regions don't include events used to measure the fake efficiencies or events included in the signal regions.

The SS regions are enriched with events with at least one non-prompt or fake lepton along with a contribution of prompt leptons from WZ and ZZ, with a small contributions from $t\bar{t}W$+jets, $t\bar{t}Z$+jets, $t\bar{t}W^+W^-$+jets and same sign $W^\pm W^\pm jj$ processes. Opposite-sign events where electron charge is misidentified, predominantly because of bremsstrahlung in the ID material followed by photon conversion, provide a significant contribution, which is estimated from the different simulated samples. Fig. 6 shows the distributions of H_{T} and of the jet multiplicity in the pretag SS validation region. The non-prompt and fake lepton contributions represent about ~35% in the $e\mu$ channel. Data and prediction show a reasonable agreement within uncertainties. Note that the uncertainty band shown does not contain the uncertainty on the MC-derived backgrounds.

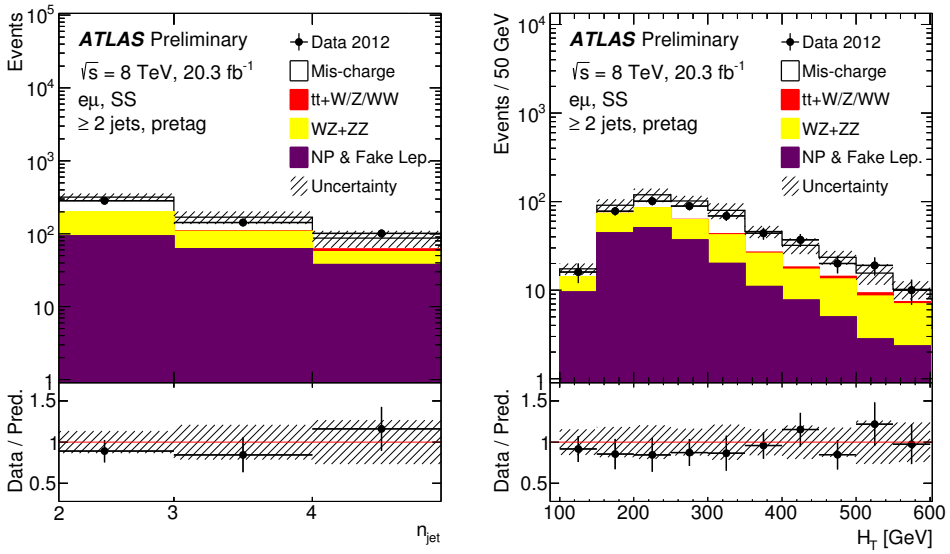

(a) (b)

Figure 6: Distribution of the jet multiplicity (a) and H_{T} (b), defined as the sum of the p_{T} of leptons and jets in the event, in the same-sign sample in the $e\mu$ channel for events with at least two jets. The data is compared to the expectation from simulation, broken down into contributions from charge-misidentification (evaluated from $t\bar{t}$, single top and Z+jets), $t\bar{t}W$+jets, $t\bar{t}Z$+jets, $t\bar{t}W^+W^-$+jets and dibosons normalised to their cross sections and non-prompt and fake lepton backrounds, referred to as 'NP & Fake Lep.', estimated with the matrix method. The shaded area represents the combination of the statistical and the systematic uncertainties on the matrix method estimate in each bin. The systematic uncertainties on the processes predicted by the MC simulation are not shown.

Fig. 7 shows the distributions of the jet multiplicity and H_{T} obtained in the $e\mu$ pretag signal region, for events with two opposite-sign charge leptons and at least two jets. The yield of non-prompt and fake lepton backgrounds is ~1%.

To further enhance the non-prompt and fake lepton contribution in this region, the corresponding validation region not-tight-tight (or !tt), where at least one of the leptons is required to fail the tight

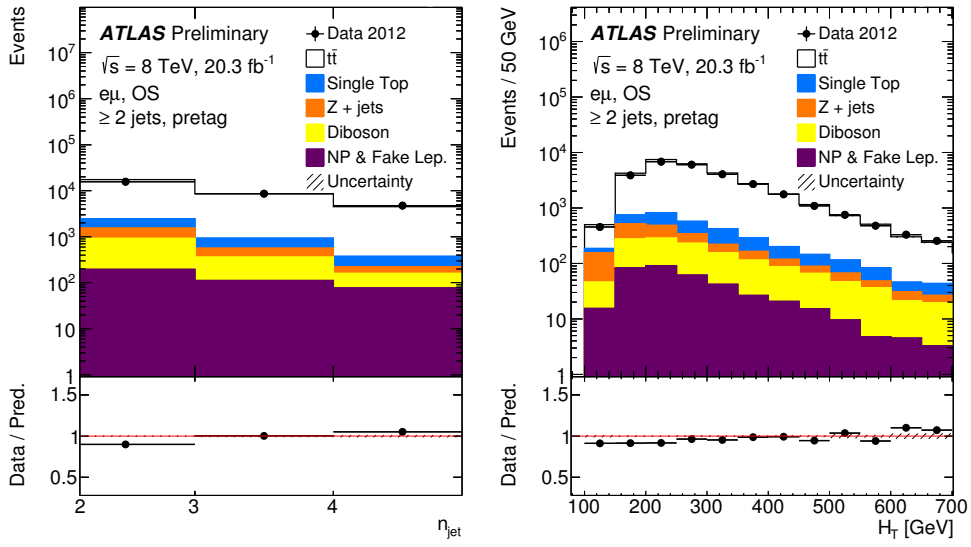

(a) (b)

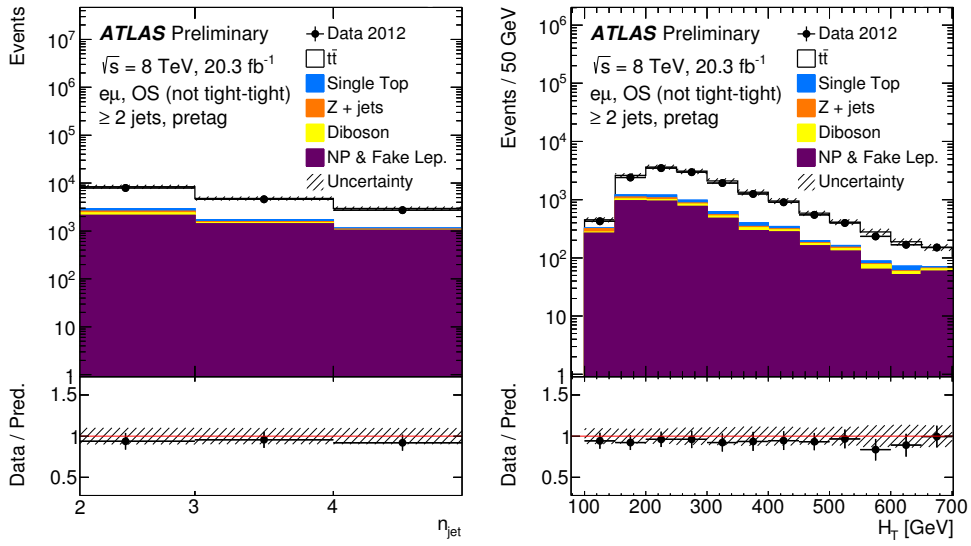

(c) (d)

Figure 7: Distribution of the jet multiplicity (a, c) and H_{T} (b, d), defined as the sum of the p_{T} of leptons and jets in the event, in the opposite-sign sample in the $e\mu$ channel for events with at least two jets. Distributions are shown for events where the two leptons are tight (a, b) and when at least one of the lepton is not tight (c, d). The data is compared to the expectation from simulation, broken down into contributions from $t\bar{t}$, single top, Z+jets and dibosons normalised to their cross sections and non-prompt and fake lepton backrounds, referred to as 'NP & Fake Lep.', estimated with the matrix method. The shaded area represents the combination of the statistical and the systematic uncertainties on the matrix method estimate in each bin. The systematic uncertainties on the processes predicted by the MC simulation are not shown.

selection, is considered. The corresponding weights to be applied become:

$$\begin{aligned} w_{\mathrm{tl}} &= \varepsilon_{r,1}\,\overline{\varepsilon_{\mathrm{f},2}}\,w_{\mathrm{rf}} + \varepsilon_{\mathrm{f},1}\,\overline{\varepsilon_{r,2}}\,w_{\mathrm{fr}} + \varepsilon_{\mathrm{f},1}\,\overline{\varepsilon_{\mathrm{f},2}}\,w_{\mathrm{ff}} \\ w_{\mathrm{lt}} &= \overline{\varepsilon_{r,1}}\,\varepsilon_{\mathrm{f},2}\,w_{\mathrm{rf}} + \overline{\varepsilon_{\mathrm{f},1}}\,\varepsilon_{r,2}\,w_{\mathrm{fr}} + \overline{\varepsilon_{\mathrm{f},1}}\,\varepsilon_{\mathrm{f},2}\,w_{\mathrm{ff}} \\ w_{\mathrm{ll}} &= \overline{\varepsilon_{r,1}}\,\overline{\varepsilon_{\mathrm{f},2}}\,w_{\mathrm{rf}} + \overline{\varepsilon_{\mathrm{f},1}}\,\overline{\varepsilon_{r,2}}\,w_{\mathrm{fr}} + \overline{\varepsilon_{\mathrm{f},1}}\,\overline{\varepsilon_{\mathrm{f},2}}\,w_{\mathrm{ff}} \\ w_{\mathrm{!tt}} &= w_{\mathrm{tl}} + w_{\mathrm{lt}} + w_{\mathrm{ll}}, \end{aligned} \tag{8}$$

The results in this region are shown in Fig. 7. The estimated non-prompt and fake lepton backgrounds are approximately 30% when at least one of the leptons is not tight.

Systematic variations on the estimates are around 50% in the validation regions with same-sign pairs, 30-50% in case of the validation regions '!tt' and 70-100% in case of the signal regions. In the opposite-sign samples the uncertainty on the real lepton efficiency dominates the systematics. In the same-sign sample, it is the uncertainty on the rate of real lepton events to subtract from MC simulation in the measurement of ε_{f} which is dominating. As in the case of the single lepton selection, data and prediction are in agreement within the systematics on the non-prompt and fake lepton background where this background is significant.

7 Fitting method

The fitting method defines a model for the non-prompt and fake leptons background shape for different distributions and performs a maximum likelihood fit to data on a discriminating variable to obtain its total normalisation. MC simulation is used to build the templates for the real lepton processes.

7.1 The jet-lepton and the anti-muon models

Two different models are defined to estimate the non-prompt and fake leptons background in e+jets and μ+jets.

In the electron channel, where jets mis-identified as electrons are an important source of background events, the jet-lepton model is defined. This model is built from a simulated di-jet sample requiring one of the jets to be electron-like, *i.e.* to fulfill the same p_{T} and η requirements as an electron and deposit 80-95% of its energy in the electromagnetic calorimeter. The jet-lepton selection is applied to simulated di-jet events to obtain the templates.

In the muon channel, the anti-muon model is used. This model is derived from data selecting a sample highly enriched in non-prompt muons. This is done by relaxing or inverting some of the muon identification cuts to select muons which are non-isolated, but still with similar kinematic properties to the ones passing the standard selection. In particular, on top of a relaxed track isolation cut, asking for $I < 0.10$ (see section 4), an inverted isolation cut is introduced, asking for the calorimeter transverse energy within a cone of $\Delta R < 0.2$ around the muon to be larger than 0.03 times the p_{T} for the muon. In addition, no longitudinal impact parameter cuts are applied.

For both models, events are selected using the same criteria as for the signal selection except for the selection of the electrons and muons. Events with additional leptons are rejected to avoid contamination from W+jets and Z+jets.

7.2 Fitting procedure

To determine the normalisation of the non-prompt and fake leptons background in each of the signal regions, a binned maximum-likelihood fit to the observed e+jets (μ+jets) data in the $E_{\mathrm{T}}^{\mathrm{miss}}$ ($m_{\mathrm{T}}^{\mathrm{W}}$) distribution is performed after applying all $t\bar{t}$ semileptonic selection criteria except for the $E_{\mathrm{T}}^{\mathrm{miss}}$ ($E_{\mathrm{T}}^{\mathrm{miss}}$ and

Table 6: Summary of the fit regions considered. The term 'pretag' is used to indicate that no requirements on the number of b-jets are applied.

Channel	n_{jet} / $n_{b-\text{jet}}$ cuts	Other cuts
e+jets	2 jets, pretag 2 jets, ≥ 1 b-tags $\geq$4 jets, pretag $\geq$4 jets, ≥ 1 b-tags	m_{T}^{W}>30 GeV
μ+jets	2 jets, pretag 2 jets, ≥ 1 b-tags $\geq$4 jets, pretag $\geq$4 jets, ≥ 1 b-tags	No cuts on $E_{\text{T}}^{\text{miss}}$, m_{T}^{W}

Table 7: Summary of the size of the Gaussian constraints applied to the real lepton templates. Values are expressed as fractions of the pre-fit yields. When labelled as 'fixed', the normalisation of the process is not allowed to vary in the fit and stays fixed to the nominal prediction. When labelled as 'free', no constraint is applied to the process.

	2 jets, pretag	2 jets, ≥ 1 b-tags	≥ 4 jets, pretag	≥ 4 jets, ≥ 1 b-tags
$t\bar{t}$, single top	fixed	10%	free	free
W+jets	free	50%	5%	fixed
Z+jets, diboson	fixed	fixed	fixed	fixed

m_{T}^{W}) requirement. Four fit regions are defined in this way and summarised in Table 6. In the electron channel two fits are performed separately, for events with the single selected electron in the barrel or in the end-cap region of the electromagnetic calorimeter, as the background composition changes between the two regions.

The non-prompt and fake leptons template is fitted together with templates derived from MC simulation for all other background processes, whose rate uncertainties are accounted for in the fitting process in the form of additional constrained nuisance parameters. The contributions from W+light-jets and $W + b\bar{b}$, $W + c\bar{c}$, $W + c$, the contributions from $t\bar{t}$ and single top-quark production, and the contributions from Z+jets and diboson production, are each combined into one template, as they show similar $E_{\text{T}}^{\text{miss}}$ and m_{T}^{W} shapes. Table 7 summarises the applied constraints in each of the signal regions and for each of the templates. In general, templates are fixed to the nominal yields if their contribution is too small to be determined in a reliable way by the fit. Templates are derived separately for different jet and b-jet multiplicities. Fig. 8 shows these template distributions for barrel e+jet and μ+jet events with at least four jets. Templates for end-cap e+jets events are not shown since they don't show a significant difference with respect to the barrel e+jet ones.

The fitting methods suffers from systematic uncertainties mainly due to the modeling of the shapes of the fit variables by the different templates. Preliminary studies to assess the effect of these uncertainties on the final estimates are based on the use of alternative fit variables and on the use of alternative simulated event samples for the most important real lepton templates. In particular, by comparing the fit results in each signal region with the results obtained by fitting the alternative distributions, specifically the m_{T}^{W} for the jet-lepton and $E_{\text{T}}^{\text{miss}}$ for the anti-muon methods, an uncertainty of 10-20% is obtained in all the signal regions except for e+jets with at least four jets, where the uncertainty is around 40%. The choice of MC generator for the W/Z+jets and $t\bar{t}$ processes (see Section 3) leads to uncertainties below 20% in all the cases, except for e+jets with at least four jets where the uncertainty is around 100%, due

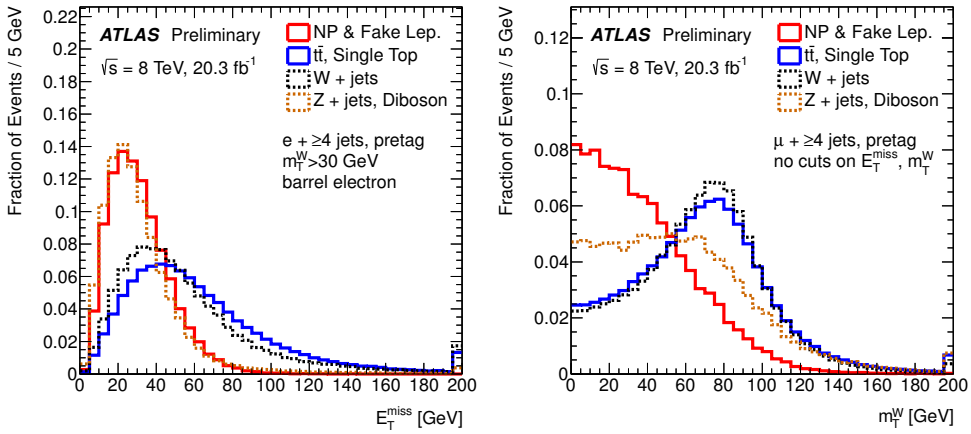

(a) (b)

Figure 8: Template distributions of $E_{\mathrm{T}}^{\mathrm{miss}}$ for events with one electron with $1.37 < |\eta_{\mathrm{cluster}}| < 1.52$ (a) or one muon (b) and at least four jets, without any b-tagging requirements, asking for $m_{\mathrm{T}}^{\mathrm{W}} > 30$ GeV in the case of e+jets and without any cuts on $E_{\mathrm{T}}^{\mathrm{miss}}$ and $m_{\mathrm{T}}^{\mathrm{W}}$ in the case of μ+jets. The templates, used for the fitting method, are obtained for real lepton processes from MC simulation and for the non-prompt and fake lepton background (referred to as 'NP & Fake Lep.') from the jet-lepton model for e+jets and anti-muon model for μ+jets (see text for details). All the templates are normalised to the same area.

to the large dependency on the $E_{\mathrm{T}}^{\mathrm{miss}}$ shape for $t\bar{t}$ events and the small fitted non-prompt and fake lepton fraction. To assess systematic uncertainties coming from the template normalisation, the size of the Gaussian constraints is changed and leads to a negligible uncertainty below 1% except for e+jets with at least four jets which is 3-8%. The effect of some other possibly important sources of uncertainties are not yet estimated for this note, in particular the systematics on the shapes of the jet-lepton and anti-muon templates, and the effect of the uncertainties on the relative fractions of the different heavy flavour components in W+jet events. These studies, together with the comparison of the predictions with data in different distribution shapes, indicate that a systematic uncertainty of 50% is representative of the overall impact of these sources. Such value is therefore used in each channel and region.

7.3 Results from the fitting method

Distributions of $E_{\mathrm{T}}^{\mathrm{miss}}$ for e+jets and $m_{\mathrm{T}}^{\mathrm{W}}$ for μ+jets events, normalised to the fit results, for events with two jets for different b-jet multiplicities are shown in Fig. 9. Good agreement is observed comparing the data to the estimated rate of non-prompt and fake lepton backgrounds summed with the other simulation predictions. In Appendix C results in fit regions with four or more jets are shown.

8 Comparison of results from the matrix method and the fitting method in lepton+jet signal regions

In the following, the techniques described in the previous sections are applied and compared in the lepton+jet signal regions, as defined in Table 2.

Detailed results are presented here for the signal region with four or more jets and no b-tag requirements. Fig. 10 and 11 show distributions of $E_{\mathrm{T}}^{\mathrm{miss}}$ and $m_{\mathrm{T}}^{\mathrm{W}}$ in e+jets and μ+jets events respectively. Non-prompt and fake lepton background estimates are obtained from the matrix method and the fitting

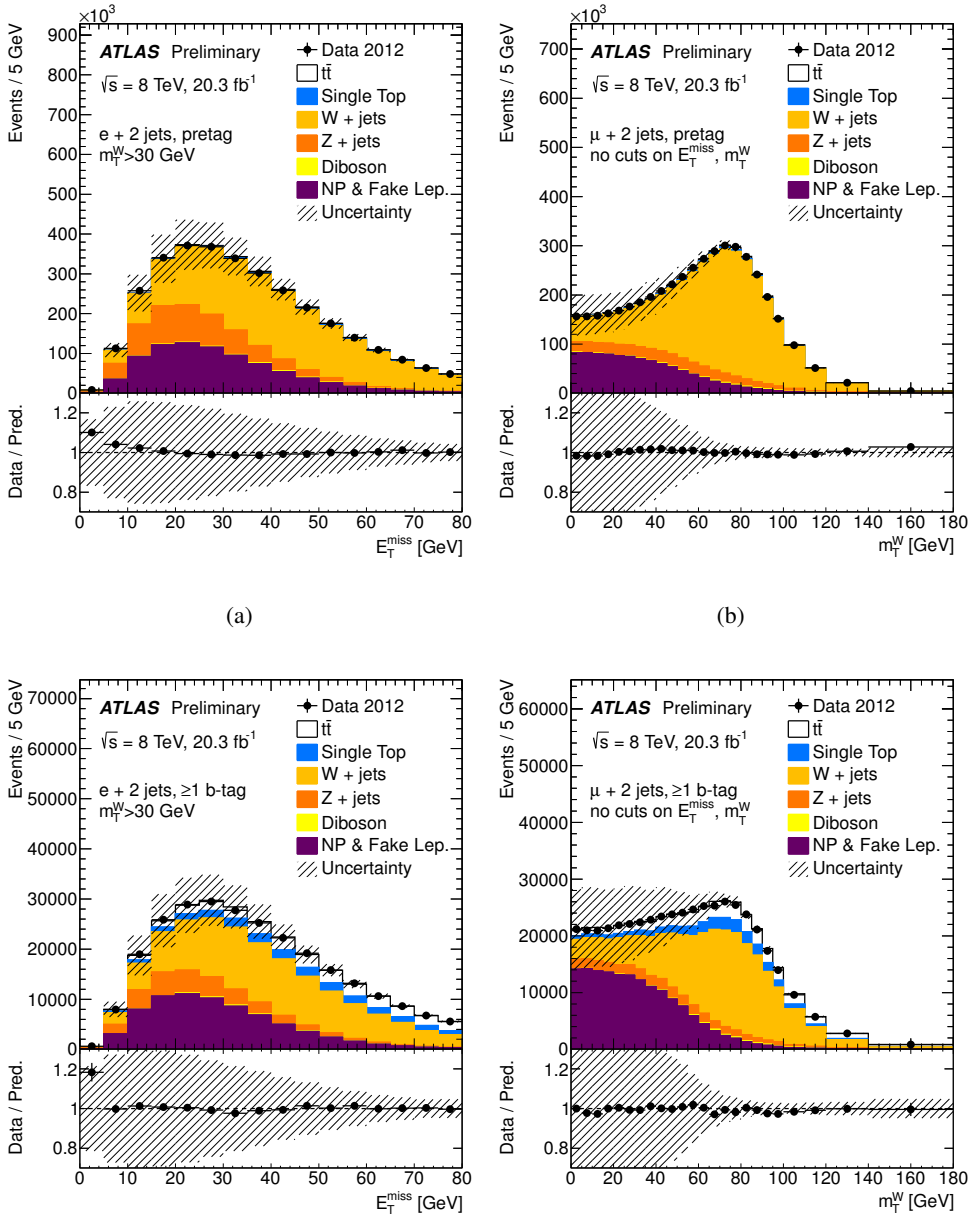

Figure 9: Distributions of $E_{\mathrm{T}}^{\mathrm{miss}}$ for e+jets (a, c) and $m_{\mathrm{T}}^{\mathrm{W}}$ for μ+jets (b, d) in events with two jets before (a, b) and after (c, d) requiring at least one b-jet, after requiring $m_{\mathrm{T}}^{\mathrm{W}}$>30 GeV in case of e+jets and without any cuts on $E_{\mathrm{T}}^{\mathrm{miss}}$ and $m_{\mathrm{T}}^{\mathrm{W}}$ in case of μ+jets. The data is compared to the expectation from simulation, showing separately the contributions from $t\bar{t}$, single top, W+jets, Z+jets and dibosons, and non-prompt and fake lepton backgrounds (referred to as 'NP & Fake Lep.') obtained form the jet-lepton and anti-muon templates, where each contribution is normalised according to the result of the application of the fitting method in each channel and region. The shaded area represents the combination of the statistical uncertainty and a 50% normalisation systematic uncertainty on the non-prompt and fake lepton estimate in each bin. The systematic uncertainties on the processes predicted by the MC simulation are not shown. Note that the good agreement between data and prediction is partially enforced here by the fact that the exact distribution used in the fit is shown.

method. In addition, Fig. 12 shows a comparison of the $E_{\mathrm{T}}^{\mathrm{miss}}$ and $m_{\mathrm{T}}^{\mathrm{W}}$ spectra as predicted by the two methods.

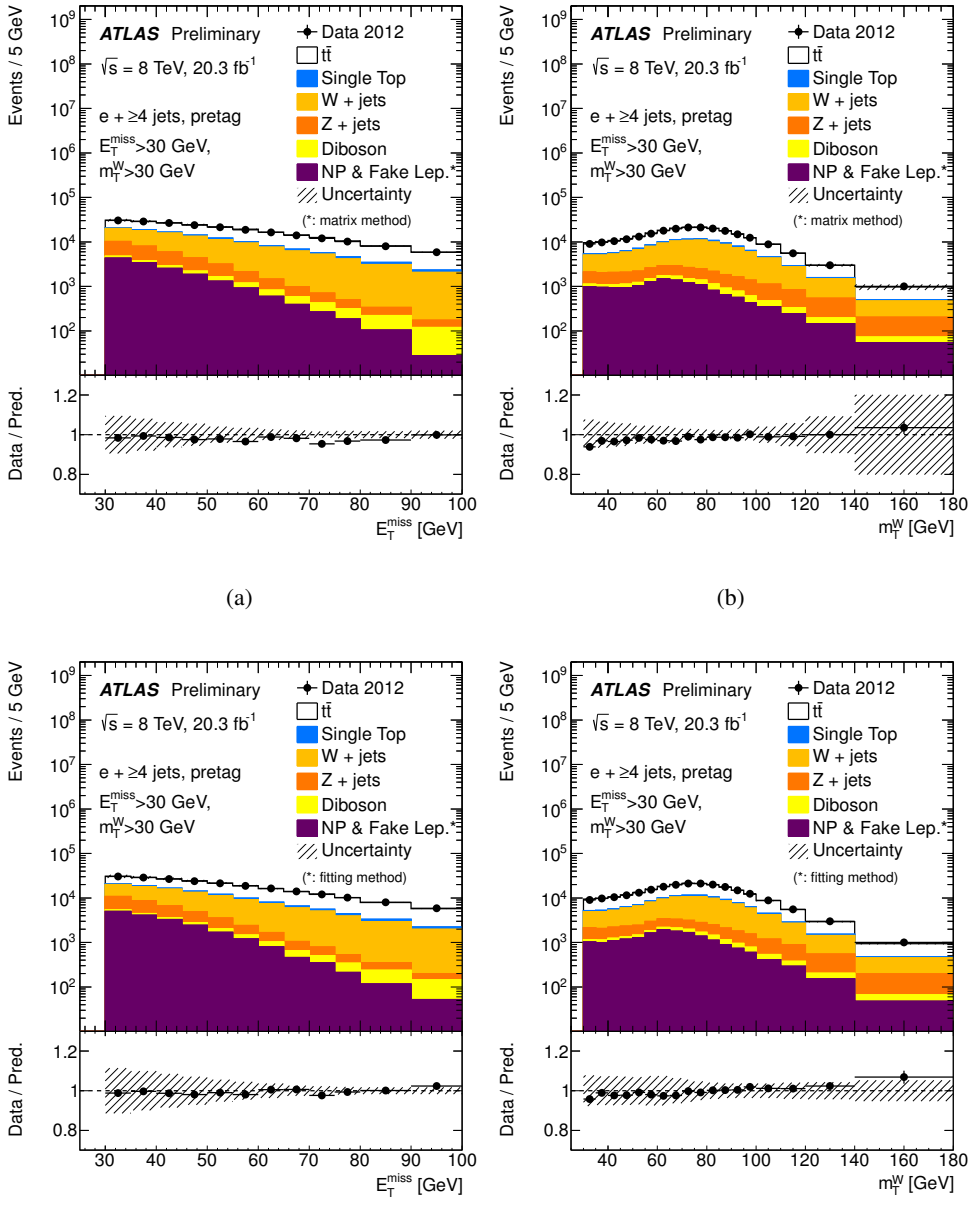

Figure 10: Distributions of $E_{\mathrm{T}}^{\mathrm{miss}}$ (a, c) and $m_{\mathrm{T}}^{\mathrm{W}}$ (b, d) for e+jets events with at least four jets without any b-tagging requirement, requiring $E_{\mathrm{T}}^{\mathrm{miss}} > 30$ GeV and $m_{\mathrm{T}}^{\mathrm{W}} > 30$ GeV. The data is shown compared to the expectation from simulation, showing separately the contributions from $t\bar{t}$, single top, W+jets, Z+jets and dibosons normalised to their cross-sections, and non-prompt and fake lepton backgrounds (referred to as 'NP & Fake Lep.') estimated with the matrix method (a, b) and with the fitting method (c, d). The shaded area represents the combination of the statistical and the systematic uncertainties on the non-prompt and fake lepton estimate in each bin. The systematic uncertainties on the processes predicted by the MC simulation are not shown.

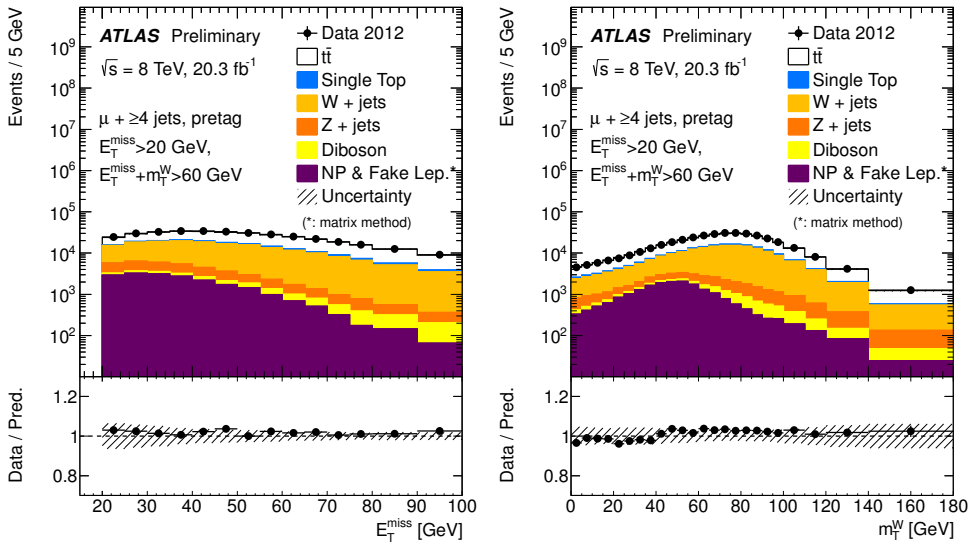

(a) (b)

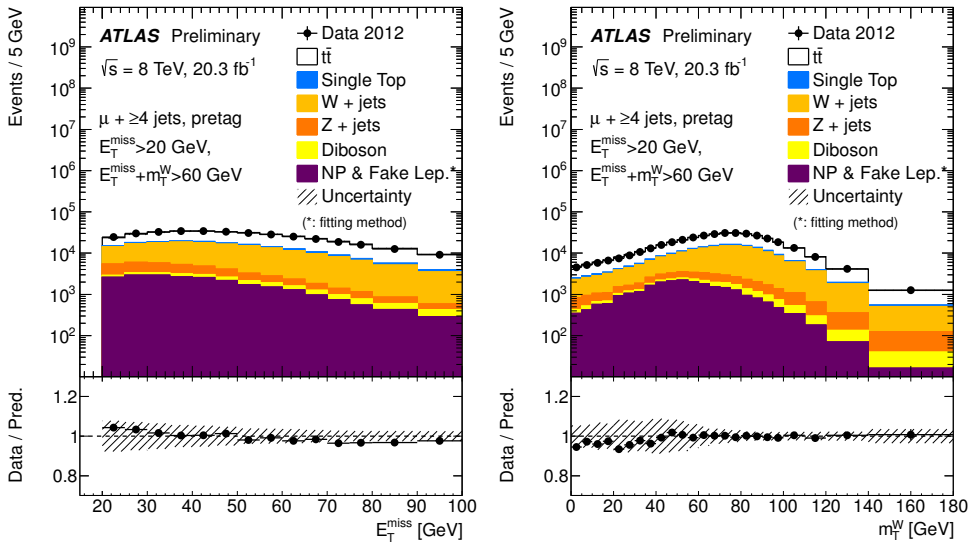

(c) (d)

Figure 11: Distributions of $E_{\mathrm{T}}^{\mathrm{miss}}$ (a, c) and $m_{\mathrm{T}}^{\mathrm{W}}$ (b, d) for μ+jets events with at least four jets without any b-tagging requirement, requiring $E_{\mathrm{T}}^{\mathrm{miss}} > 20$ GeV and $E_{\mathrm{T}}^{\mathrm{miss}} + m_{\mathrm{T}}^{\mathrm{W}} > 60$ GeV. The data is shown compared to the expectation from simulation, showing separately the contributions from $t\bar{t}$, single top, W+jets, Z+jets and dibosons normalised to their cross-sections, and non-prompt and fake lepton backgrounds (referred to as 'NP & Fake Lep.') estimated with the matrix method (a, b) and with the fitting method (c, d). The shaded area represents the combination of the statistical and the systematic uncertainties on the non-prompt and fake lepton estimate in each bin. The systematic uncertainties on the processes predicted by the MC simulation are not shown.

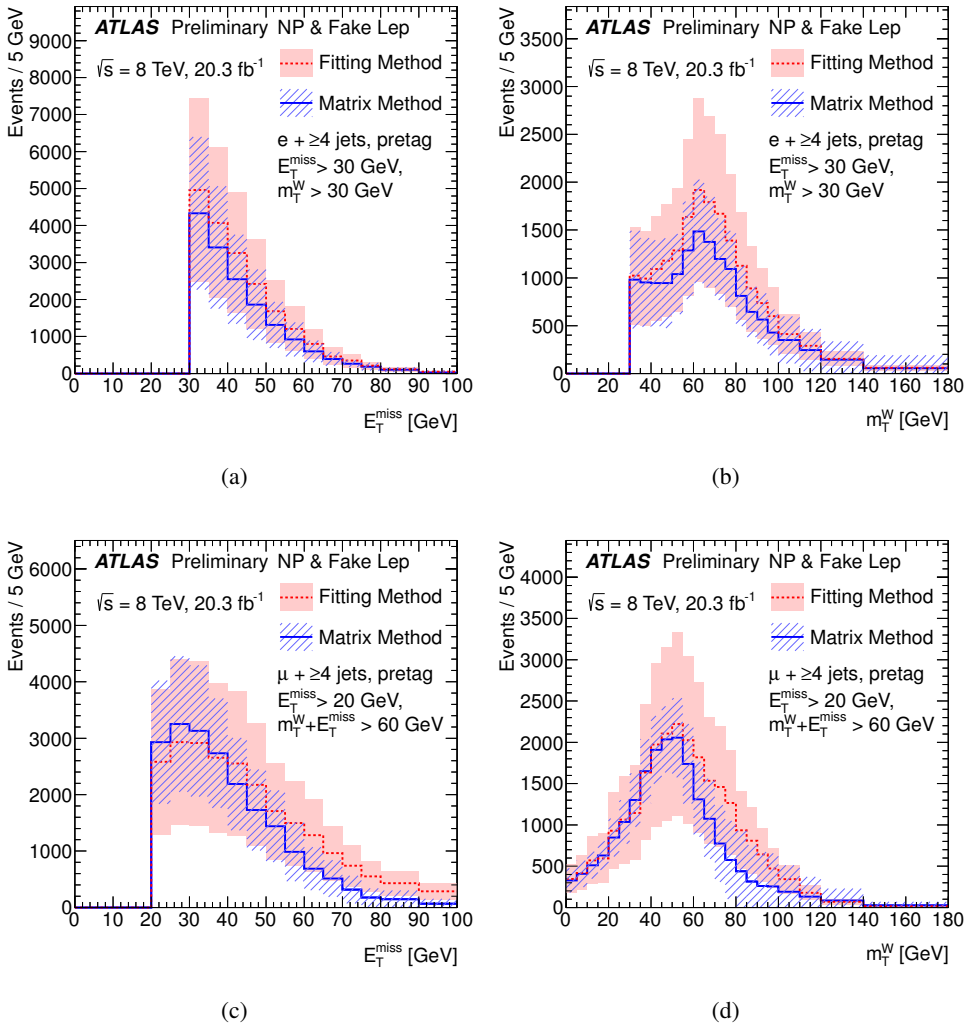

Figure 12: Comparison of the non-prompt and fake lepton background predictions by the matrix method and the fit methods, in terms of $E_{\mathrm{T}}^{\mathrm{miss}}$ (a, c) and $m_{\mathrm{T}}^{\mathrm{W}}$ (b, d) distributions in the e+jets (a, b) and μ+jets (c, d) channels, for events with at least four jets, without any b-tagging requirement, asking for $E_{\mathrm{T}}^{\mathrm{miss}} > 30$ GeV and $m_{\mathrm{T}}^{\mathrm{W}} > 30$ GeV in case of e+jets and $E_{\mathrm{T}}^{\mathrm{miss}} > 20$ GeV and $E_{\mathrm{T}}^{\mathrm{miss}} + m_{\mathrm{T}}^{\mathrm{W}} > 60$ GeV in case of μ+jets. The shaded area represents, for each of the two methods, the total uncertainty on the estimate in each bin.

Fig. 13 shows a comparison of the predicted yields in all the lepton+jet signal regions with and without asking for at least one b-tagged jet. The two estimates are in agreement within the systematic uncertainties.

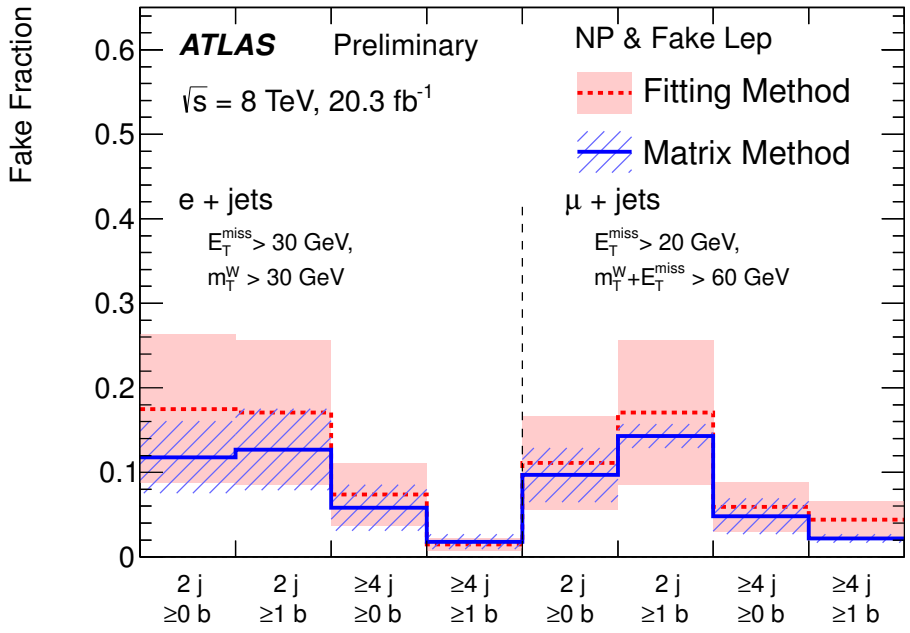

Figure 13: Comparison of the non-prompt and fake lepton background predictions by the matrix method and the fit method divided by the number of observed events (referred to as 'Fake Fraction') in each of the lepton+jet signal regions in the e+jets and μ+jets channels. The shaded area represents the total uncertainties on the two methods in each region.

9 Conclusion

Two methods for estimating non-prompt and fake lepton backgrounds for top analyses are presented using 20.3 fb^{-1} of data collected in 2012 by the ATLAS detector with proton-proton collisions at the LHC. These backgrounds are estimated using two independent methods. For final states with two leptons, the matrix method is used and the systematic uncertainties of the estimates are between 30 and 100%. For final states with one lepton, results obtained using the matrix method and the fitting method are compared and give consistent results within systematic uncertainties, which are between 10 and 50% for the matrix method and 50% for the fitting method.

References

[1] ATLAS Collaboration, *Measurement of the top quark pair production cross-section with ATLAS in pp collisions at* $\sqrt{s}$ = 7 *TeV*, Eur. Phys. J C **71** (2011) 1577, arXiv:1012.1792 [hep-ex].

[2] ATLAS Collaboration, *Measurement of the cross section for top-quark pair production in pp collisions at* $\sqrt{s}$*=7 TeV with the ATLAS detector using final states with two high-pt leptons*, JHEP **1205** (2012) 059, arXiv:1202.4892 [hep-ex].

[3] ATLAS Collaboration, *Simultaneous measurements of the* $t\bar{t}$*,* W^+W*, and* $Z/\gamma^* \to \tau\tau$ *production cross-sections in pp collisions at* $\sqrt{s}$*=7 TeV with the ATLAS detector*, arXiv:1407.0573 [hep-ex]. Submitted to PRD.

[4] ATLAS Collaboration, *Comprehensive measurements of t-channel single top-quark production cross sections at* $\sqrt{s}$*=7 TeV with the ATLAS detector*, arXiv:1406.7844 [hep-ex]. Submitted to PRD.

[5] ATLAS Collaboration, *Measurement of the* $t\bar{t}$ *production cross-section using* $e\mu$ *events with b-tagged jets in pp collisions at* $\sqrt{s}$ = 7 *and* 8 *TeV with the ATLAS detector*, arXiv:1406.5375 [hep-ex]. Submitted to EPJC.

[6] ATLAS Collaboration, *Evidence for the associated production of a vector boson (W, Z) and top quark pair in the dilepton and trilepton channels in pp collision data at* $\sqrt{s}$ = 8 *TeV collected by the ATLAS detector at the LHC*, ATLAS-CONF-2014-038. http://cds.cern.ch/record/1735215.

[7] ATLAS Collaboration, *The ATLAS detector at the LHC*, JINST **3** (2008) S08003.

[8] P. Nason, *A New method for combining NLO QCD with shower Monte Carlo algorithms*, JHEP **0411** (2004) 040, arXiv:hep-ph/0409146 [hep-ph].

[9] S. Frixione, P. Nason and C. Oleari, *Matching NLO QCD computations with parton shower simulations: the POWHEG method*, JHEP **11** (2007) 070, arXiv:0709.2092 [hep-ph].

[10] H1 and ZEUS Collaboration Collaboration, F. D. Aaron et al., *Combined Measurement and QCD Analysis of the Inclusive e+- p Scattering Cross Sections at HERA*, JHEP **1001** (2010) 109, arXiv:0911.0884 [hep-ex].

[11] T. Sjöstrand et al., *High-energy-physics event generation with Pythia-6.1*, Comput. Phys. Commun. **135** (2001) no.2, 238.

[12] P. Z. Skands, *Tuning Monte Carlo Generators: The Perugia Tunes*, Phys. Rev. D **82** (2010) 074018, arXiv:1005.3457 [hep-ph].

[13] ATLAS Collaboration, *Comparison of Monte Carlo generator predictions for gap fraction and jet multiplicity observables in* $t\bar{t}$ *events*, ATL-PHYS-PUB-2014-005. http://cds.cern.ch/record/1703034.

[14] H.-L. Lai et al., *New parton distributions for collider physics*, Phys.Rev. **D82** (2010) 074024, arXiv:1007.2241 [hep-ph].

[15] ATLAS Collaboration, *ATLAS tunes of PYTHIA 6 and Pythia 8 for MC11*, ATL-PHYS-PUB-2011-009. http://cds.cern.ch/record/1363300.

[16] M. Cacciari et al., *Top-pair production at hadron colliders with next-to-next-to-leading logarithmic soft-gluon resummation*, Phys.Lett. **B710** (2012) 612–622, arXiv:1111.5869 [hep-ph].

[17] M. Beneke, P. Falgari, S. Klein, and C. Schwinn, *Hadronic top-quark pair production with NNLL threshold resummation*, Nucl.Phys. **B855** (2012) 695–741, arXiv:1109.1536 [hep-ph].

[18] P. Baernreuther, M. Czakon, and A. Mitov, *Percent Level Precision Physics at the Tevatron: First Genuine NNLO QCD Corrections to $q\bar{q} \to t\bar{t} + X$*, Phys.Rev.Lett. **109** (2012) 132001, arXiv:1204.5201 [hep-ph].

[19] M. Czakon and A. Mitov, *NNLO corrections to top pair production at hadron colliders: the quark-gluon reaction*, JHEP **1301** (2013) 080, arXiv:1210.6832 [hep-ph].

[20] M. Czakon, P. Fiedler, and A. Mitov, *The total top quark pair production cross-section at hadron colliders through $O(\alpha_S^4)$*, Phys. Rev. Lett. **110** (2013) 252004, arXiv:1303.6254 [hep-ph].

[21] M. Czakon and A. Mitov, *NNLO corrections to top-pair production at hadron colliders: the all-fermionic scattering channels*, JHEP **1212** (2012) 054, arXiv:1207.0236 [hep-ph].

[22] M. Czakon and A. Mitov, *Top++: A Program for the Calculation of the Top-Pair Cross-Section at Hadron Colliders*, Comp. Phys. Commun. **185** (2014) 2930, arXiv:1112.5675 [hep-ph].

[23] M. Botje et al., *The PDF4LHC Working Group Interim Recommendations*, arXiv:1101.0538 [hep-ph].

[24] A. Martin, W. Stirling, R. Thorne, and G. Watt, *Parton distributions for the LHC*, Eur.Phys.J. **C63** (2009) 189–285, arXiv:0901.0002 [hep-ph].

[25] A. Martin, W. Stirling, R. Thorne, and G. Watt, *Uncertainties on alpha(S) in global PDF analyses and implications for predicted hadronic cross sections*, Eur.Phys.J. **C64** (2009) 653–680, arXiv:0905.3531 [hep-ph].

[26] J. Gao et al., *The CT10 NNLO Global Analysis of QCD*, Phys. Rev. D **89** (2014) 033009, arXiv:1302.6246 [hep-ph].

[27] R. Ball et al., *Parton distributions with LHC data*, Nucl.Phys. **B867** (2013) 244–289, arXiv:1207.1303 [hep-ph].

[28] B.P. Kersevan and E. Richter-Wąs, *The Monte Carlo event generator AcerMC version 2.0 with interfaces to PYTHIA 6.2 and HERWIG 6.5*, (2004) , arXiv:hep-ph/0405247.

[29] S. Frixione, E. Laenen, P. Motylinski, and B. R. Webber, *Single-top production in MC@NLO*, JHEP **0603** (2006) 092, arXiv:hep-ph/0512250 [hep-ph].

[30] N. Kidonakis, *Two-loop soft anomalous dimensions for single top quark associated production with a W^- or H^-*, Phys. Rev. D **82** (2010) 054018, arXiv:1005.4451 [hep-ph].

[31] N. Kidonakis, *Next-to-next-to-leading-order collinear and soft gluon corrections for t-channel single top quark production*, Phys. Rev. D **83** (2011) 091503, arXiv:1103.2792 [hep-ph].

[32] M. L. Mangano, M. Moretti, F. Piccinini, R. Pittau, and A. D. Polosa,, *ALPGEN, a generator for hard multiparton processes in hadronic collisions*, JHEP **07** (2003) 001, arXiv:hep-ph/0206293 [hep-ph].

[33] P. M. Nadolsky et al., *Implications of CTEQ global analysis for collider observables*, Phys. Rev. D **78** (2008) 013004, arXiv:0802.007 [hep-ph].

[34] M. L. Mangano et al., *Multijet matrix elements and shower evolution in hadronic collisions: $Wb\bar{b}$+n jets as a case study*, Nucl. Phys. B **632** (2002) 343, arXiv:hep-ph/0108069 [hep-ph].

[35] T. Gleisberg et al., *Event generation with SHERPA 1.1*, JHEP **02** (2009) 007, arXiv:0811.4622 [hep-ph].

[36] C. Anastasiou, L. J. Dixon, K. Melnikov, and F. Petriello, *High precision QCD at hadron colliders: Electroweak gauge boson rapidity distributions at NNLO*, Phys. Rev. D **69** (2004) 094008, arXiv:hep-ph/0312266.

[37] F. A. Berends, H. Kuijf, B. Tausk, and W. T. Giele, *On the Production of a W and Jets at Hadron Colliders*, Nucl. Phys. B **357** (1991) 32–64.

[38] S. D. Ellis, R. Kleiss, and W. J. Stirling, *Ws, Zs and Jets*, Phys. Lett. B **154** (1985) 435.

[39] J. Alwall et al, *MadGraph/MadEvent v4: the new web generation*, JHEP **09** (2007) 028, arXiv:0706.2334 [hep-ph].

[40] T. Sjöstrand, S. Mrenna, and P. Z. Skands, *A Brief Introduction to PYTHIA 8.1*, Comput. Phys. Commun. **178** (2008) 852, arXiv:0710.3820 [hep-ph].

[41] P. Golonka and Z. Wąs, *PHOTOS Monte Carlo: a precision tool for QED corrections in Zand Wdecays*, Eur. Phys. J C **45** (2006) 97, arXiv:hep-ph/0506026 [hep-ph].

[42] S. Jadach, J. H. Kühn, and Z. Wąs, *TAUOLA - a library of Monte Carlo programs to simulate decays of polarized τ leptons*, Comput. Phys. Commun. **64** (1991) 275.

[43] ATLAS Collaboration, *The ATLAS Simulation Infrastructure*, Eur. Phys. J C **70** (2010) 823–874, arXiv:1005.4568 [physics.ins-det].

[44] GEANT4 Collaboration, S. Agostinelli et al., *GEANT4 - A Simulation Toolkit*, Nucl. Instr. and Meth. **A506** (2003) 250.

[45] ATLAS Collaboration, *Electron reconstruction and identification efficiency measurements with the ATLAS detector using the 2011 LHC proton-proton collision data*, Eur. Phys. J C **74** (2014) 2941, arXiv:1404.2240 [hep-ex].

[46] ATLAS Collaboration, *Measurement of the muon reconstruction performance of the ATLAS detector using 2011 and 2012 LHC proton-proton collision data*, arXiv:1407.3935 [hep-ex]. Submitted to Eur. Phys. J. C.

[47] M. Cacciari and G. P. Salam, *Dispelling the N^3 myth for the kt jet-finder*, Physics Letters B **641** no. 1, (2006) 57 – 61.

[48] M. Cacciari, G. P. Salam, and G. Soyez, *The anti-kt jet clustering algorithm*, JHEP **04** (2008) 063, arXiv:0802.1189 [hep-ph].

[49] ATLAS Collaboration, *Jet energy measurement with the ATLAS detector in proton-proton collisions at $\sqrt{s} = 7$ TeV*, Eur. Phys. J C **73 3** (2013) 2304, arXiv:1112.6426 [hep-ex].

[50] ATLAS Collaboration, *Commissioning of the ATLAS high-performance b-tagging algorithms in the 7 TeV collision data*, ATLAS-CONF-2011-102. http://cds.cern.ch/record/1369219.

[51] ATLAS Collaboration, *Calibration of b-tagging using dileptonic top pair events in a combinatorial likelihood approach with the ATLAS experiment*, ATLAS-CONF-2014-004. http://cds.cern.ch/record/1664335.

[52] ATLAS Collaboration, *b-jet tagging calibration on c-jets containing D mesons*, ATLAS-CONF-2012-039. https://cds.cern.ch/record/1435193.

[53] ATLAS Collaboration, *Measurement of the Mistag Rate of b-tagging algorithms with 5 fb^{-1} of Data Collected by the ATLAS Detector*, ATLAS-CONF-2012-040. https://cds.cern.ch/record/1435194.

[54] ATLAS Collaboration, *Performance of missing transverse momentum reconstruction in proton-proton collisions at 7 TeV with ATLAS*, Eur. Phys. J C **72** (2012) 1844, arXiv:1108.5602 [hep-ex].

[55] ATLAS Collaboration, *Measurements of spin correlation in top-antitop quark events from proton-proton collisions at $\sqrt{s} = 7$ using the ATLAS detector*, arXiv:1407.4314 [hep-ex]. Submitted to PRD.

[56] ATLAS Collaboration, *Measurement of the top quark pair production cross section in the single-lepton channel with ATLAS in proton-proton collisions at 8 TeV using kinematic fits with b-tagging*, ATLAS-CONF-2012-149. http://cds.cern.ch/record/1493488.

A Additional figures on matrix method efficiencies

Figure 14 shows the dilepton invariant mass distributions used to extract the real efficiencies for the matrix method for electrons and muons.

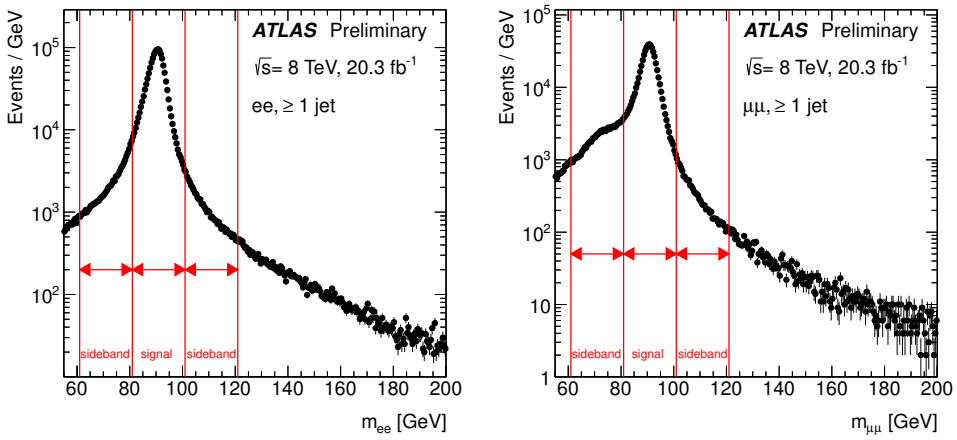

(a) (b)

Figure 14: Distribution of the invariant mass of opposite sign charge electron (a) and muon (b) pairs. Events with one tight and one loose lepton and at least one jet are selected. Lines show the signal and sideband regions from which the yields are calculated.

B Additional matrix method validation region figures

Fig. 15 and 16 show the matrix method results in the validation regions with four or more jets.

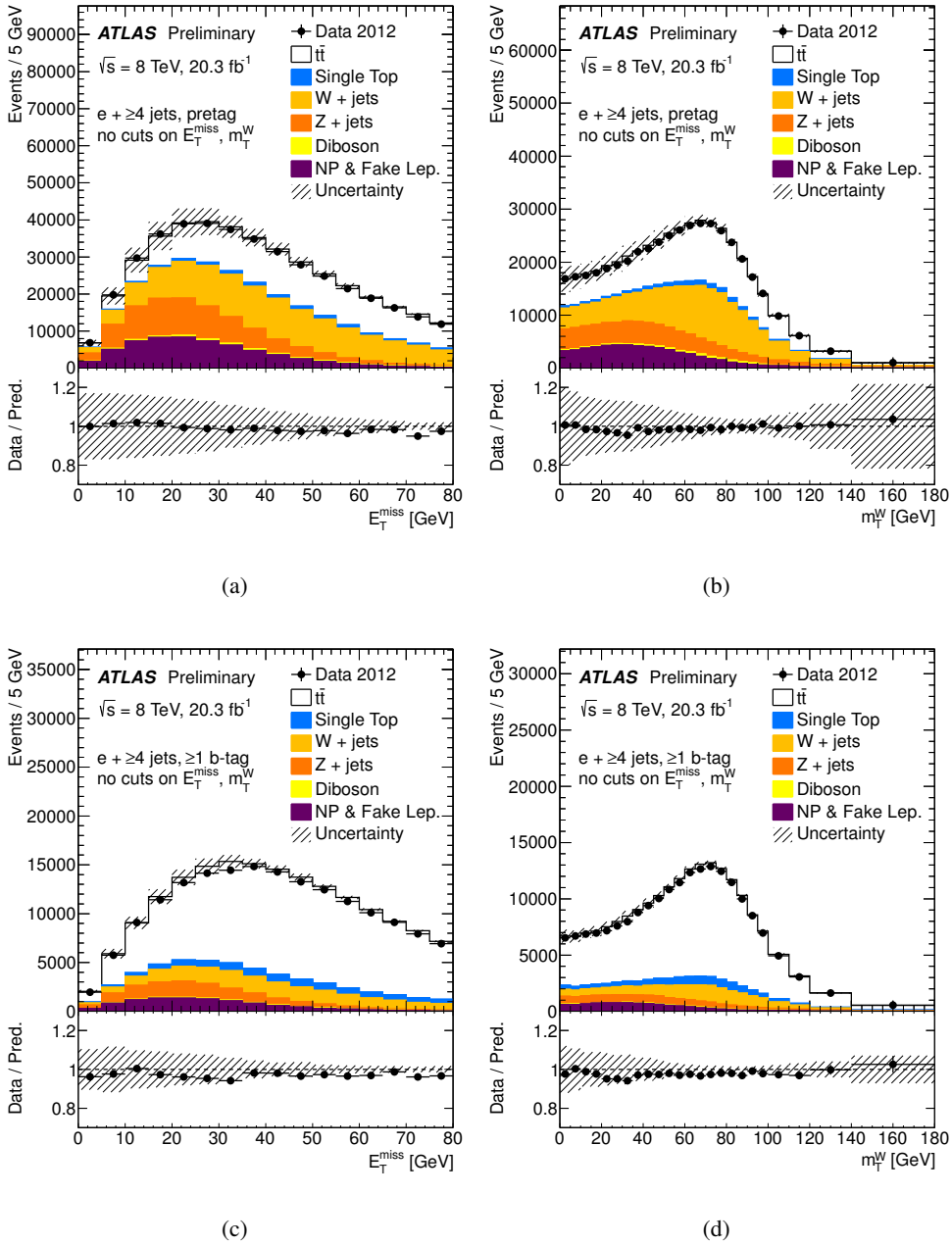

Figure 15: Distributions of $E_{\mathrm{T}}^{\mathrm{miss}}$ (a, c) and $m_{\mathrm{T}}^{\mathrm{W}}$ (b, d) in e+jets events with at least four jets before (a, b) and after (c, d) requiring at least one b-jet, without any cuts on $E_{\mathrm{T}}^{\mathrm{miss}}$ and $m_{\mathrm{T}}^{\mathrm{W}}$. The data is compared to the expectation from simulation, showing separately the contributions from $t\bar{t}$, single top, W+jets, Z+jets and dibosons normalised to their cross-sections, and non-prompt and fake lepton backgrounds (referred to as 'NP & Fake Lep.') estimated with the matrix method. The shaded area represents the combination of the statistical and the systematic uncertainties on the matrix method estimate in each bin. The systematic uncertainties on the processes predicted by the MC simulation are not shown.

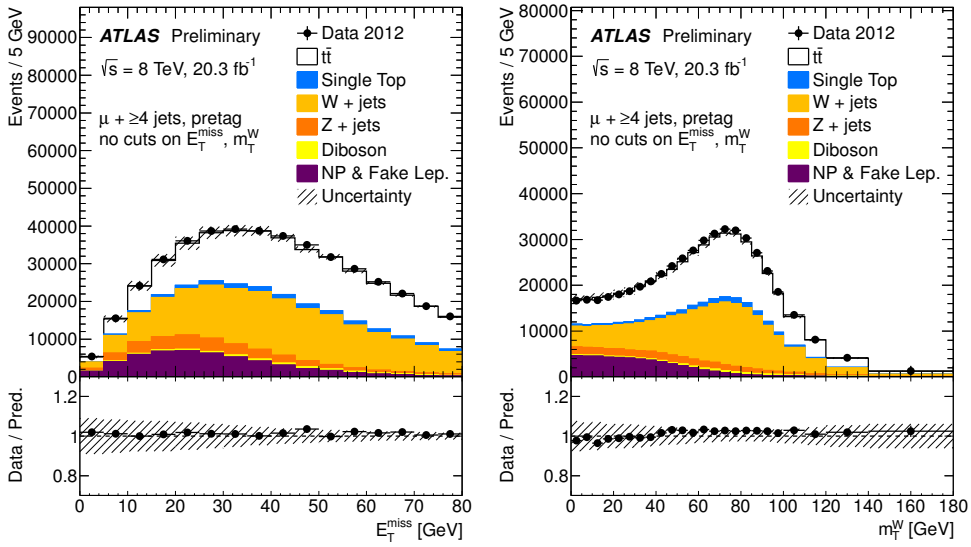

(a) (b)

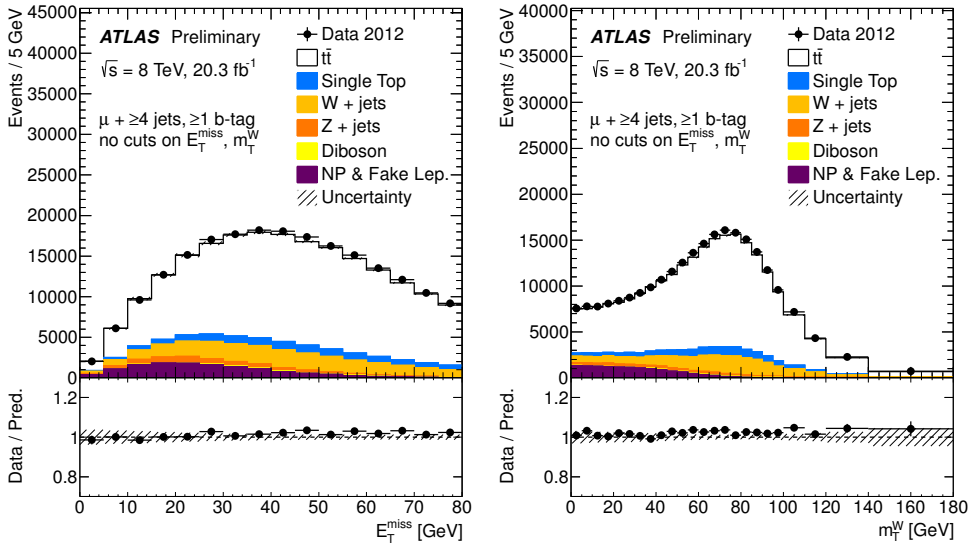

(c) (d)

Figure 16: Distributions of $E_{\mathrm{T}}^{\mathrm{miss}}$ (a, c) and $m_{\mathrm{T}}^{\mathrm{W}}$ (b, d) in μ+jets events with at least four jets before (a, b) and after (c, d) requiring at least one b-jet, without any cuts on $E_{\mathrm{T}}^{\mathrm{miss}}$ and $m_{\mathrm{T}}^{\mathrm{W}}$. The data is compared to the expectation from simulation, showing separately the contributions from $t\bar{t}$, single top, W+jets, Z+jets and dibosons normalised to their cross-sections, and non-prompt and fake lepton backgrounds (referred to as 'NP & Fake Lep.') estimated with the matrix method. The shaded area represents the combination of the statistical and the systematic uncertainties on the matrix method estimate in each bin. The systematic uncertainties on the processes predicted by the MC simulation are not shown.

C Additional fit region figures

Fig. 17 shows plots in the fit regions with four or more jets.

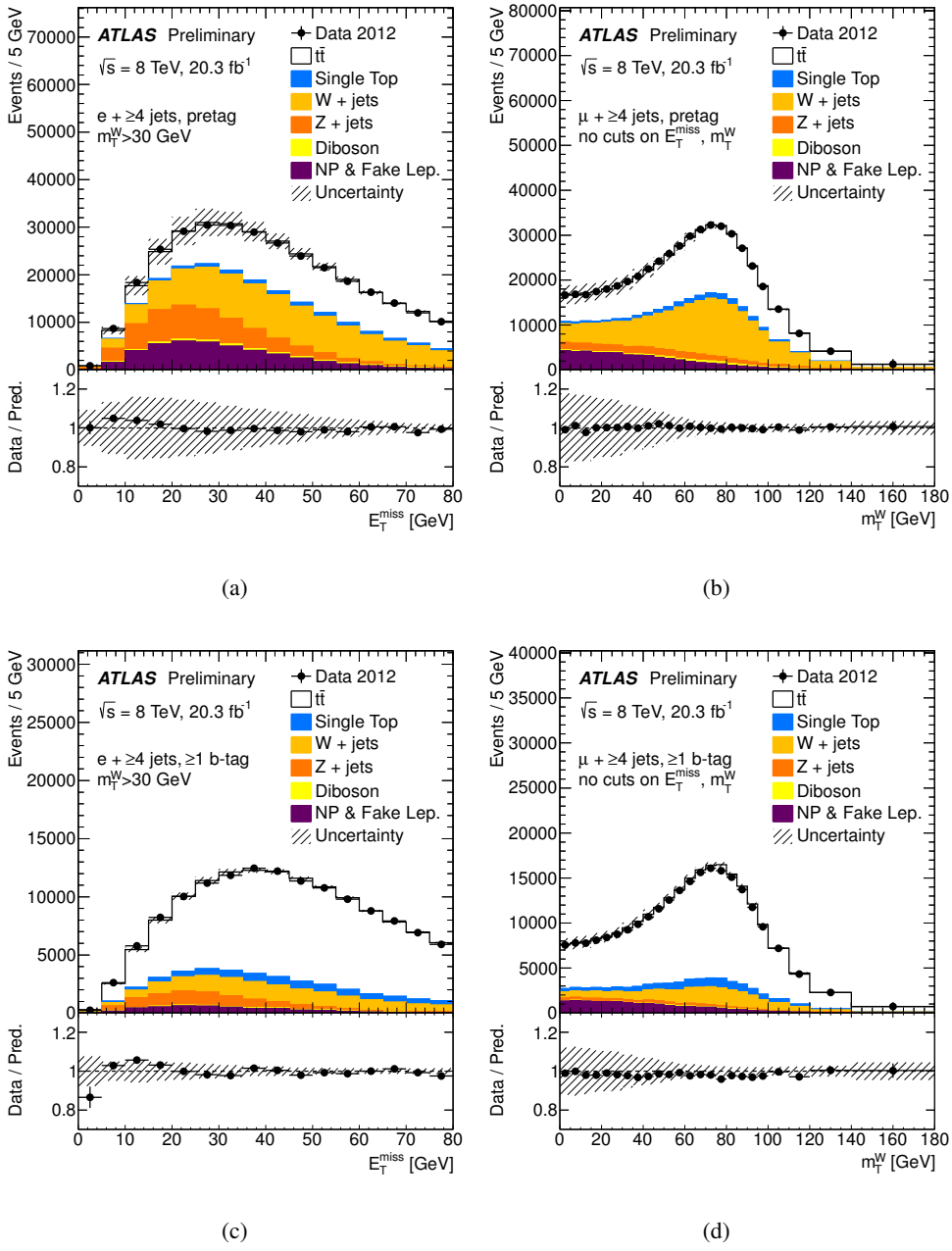

Figure 17: Distributions of $E_{\mathrm{T}}^{\mathrm{miss}}$ for e+jets (a, c) and $m_{\mathrm{T}}^{\mathrm{W}}$ for μ+jets (b, d) in events with at least four jets before (a, b) and after (c, d) requiring at least one b-jet, after requiring $m_{\mathrm{T}}^{\mathrm{W}}$>30 GeV in case of e+jets and without any cuts on $E_{\mathrm{T}}^{\mathrm{miss}}$ and $m_{\mathrm{T}}^{\mathrm{W}}$ in case of μ+jets. The data is compared to the expectation from simulation, showing separately the contributions from $t\bar{t}$, single top, W+jets, Z+jets and dibosons, and non-prompt and fake lepton backgrounds (referred to as 'NP & Fake Lep.') obtained form the jet-lepton and anti-muon templates, where each contribution is normalised according to the result of the application of the fitting method in each channel and region. The shaded area represents the combination of the statistical uncertainty and a 50% normalisation systematic uncertainty on the non-prompt and fake lepton estimate in each bin. The systematic uncertainties on the processes predicted by the MC simulation are not shown. Note that the good agreement between data and prediction is partially enforced here by the fact that the exact distribution used in the fit is shown.